Magnetocaloric effect and its relation to shape-memory properties in ferromagnetic Heusler alloys

2009 J. Phys.: Condens. Matter 21 233201

(http://iopscience.iop.org/0953-8984/21/23/233201)

J. Phys.: Condens. Matter **21** (2009) 233201 (29pp) doi:10.1088/0953-8984/21/23/233201

TOPICAL REVIEW

Magnetocaloric effect and its relation to shape-memory properties in ferromagnetic Heusler alloys

Antoni Planes[1], **Lluís Mañosa**[1] **and Mehmet Acet**[2]

[1] Departament d'Estructura i Constituents de la Matèria, Facultat de Física, Universitat de Barcelona, Diagonal 647, E-08028 Barcelona, Catalonia, Spain
[2] Experimentalphysik, Universität Duisburg-Essen, D-47048 Duisburg, Germany

E-mail: toni@ecm.ub.es, lluis@ecm.ub.es and mehmet.acet@uni-due.de

Received 19 December 2008, in final form 21 April 2009
Published 18 May 2009
Online at stacks.iop.org/JPhysCM/21/233201

Abstract
Magnetic Heusler alloys which undergo a martensitic transition display interesting functional properties. In the present review, we survey the magnetocaloric effects of Ni–Mn-based Heusler alloys and discuss their relation with the magnetic shape-memory and magnetic superelasticity reported in these materials. We show that all these effects are a consequence of a strong coupling between structure and magnetism which enables a magnetic field to rearrange martensitic variants as well as to provide the possibility to induce the martensitic transition. These two features are respectively controlled by the magnetic anisotropy of the martensitic phase and by the difference in magnetic moments between the structural phases. The relevance of each of these contributions to the magnetocaloric properties is analysed.

(Some figures in this article are in colour only in the electronic version)

Contents

1. Introduction

Magnetocaloric effects occur in any magnetic material due to the interdependence of thermal and magnetic properties. They are commonly induced by the application or removal of an external magnetic field and measured as a temperature change when the field is adiabatically swept, or as an entropy change when the process is isothermal [1]. This long-standing, well-known phenomenon has been widely used in the past for low-temperature cryogenic applications. Changes of temperature in iron induced by a magnetic field were originally reported by Warburg already in 1881 [2]. However, only in the late 1920s Debye [3] and Giauque [4] independently proposed an interpretation based on thermodynamics and suggested the possibility of cooling by adiabatic demagnetization. Such an interpretation was experimentally proved a few years later by Giauque and MacDougall [5]. In recent years, the discovery of the giant magnetocaloric response in $Gd_5(Si_xGe_{1-x})_4$ [6] has stimulated both basic and applied interest in the development of new materials that are useful for room temperature magnetic refrigeration as an alternative to vapour-compression technology [7].

Among new magnetocaloric materials, an interesting class are Heusler materials [8]. These are ordered intermetallics with the generic formula X_2YZ in which the three components occupy the crystallographically non-equivalent positions of an $L2_1$ structure. X and Y are 3d elements and Z is a group IIIA–VA element. These alloys show magnetism which is due to the X and/or Y elements. Although they are metals, the magnetic properties can often be described in terms of localized magnetic moments with indirect exchange interactions. In the important Ni–Mn-based family, the magnetic moment is confined to the Mn atoms to a large extent.

The present review focuses on those Heusler alloys undergoing a structural (martensitic) transition which involves a change in both structural and magnetic properties of the solid. Associated with this first-order magnetostructural transition, these materials display shape-memory properties including magnetic shape-memory and superelastic effects. Magnetic shape-memory properties were first discovered in 1996 [9]. The prototype material is Ni–Mn–Ga in a composition range close to the 2–1–1 Heusler stoichiometry. A few years later, it was shown that these materials also display interesting magnetocaloric properties in the vicinity of the martensitic transition [10, 11]. The first investigations [10] were carried out on Ni–Mn–Ga alloy undergoing a martensitic transition below 200 K for which a positive entropy change (inverse effect) was observed for an applied field below 1 T. Surprisingly enough, in a further investigation [11], a negative entropy change (conventional effect) was reported for fields above 1 T for an alloy of slightly different composition transforming near 290 K. The explanation of the different magnetocaloric behaviours was provided in [12, 13], where it was shown that an inverse effect taking place at low fields was related to the strong uniaxial magnetocrystalline anisotropy of the martensitic phase. When the composition is varied in such a way that the martensitic transition temperature approaches the Curie temperature, the anisotropy weakens with a corresponding decrease of the inverse contribution and conventional behaviour becomes dominant. Actually, optimum magnetocaloric properties were shown to occur when both the martensitic and ferromagnetic transitions occur close to one another [14].

More recently, other Ni–Mn-based Heusler alloys have been shown to exhibit large magnetocaloric effects. As opposed to the case of Ni–Mn–Ga mentioned above, these alloys exhibit an inverse effect for all studied magnetic fields. The inverse magnetocaloric effect has previously been reported at the antiferromagnetic–ferromagnetic phase transition in Fe–Rh [15]. However, a particular feature of Ni–Mn-based Heusler alloys is that the large inverse magnetocaloric effect relies on a structural transition, with the two structures being predominantly ferromagnetic [16].

In the following, we begin by discussing thermodynamics of general caloric effects with emphasis on magnetocaloric effects in the vicinity of first-order magnetostructural transitions. We next focus on the structural and magnetic properties of Ni–Mn-based martensitic Heusler alloys, giving details of their volumetric and electronic aspects. Shape-memory and magnetocaloric properties in these systems are closely related to one another. Therefore, we finally discuss the details of these properties and their relationship to one another in Ni–Mn-based Heusler alloys.

2. Thermodynamics of magnetocaloric effect

Caloric effects occur in any macroscopic physical system as a consequence of its thermal response to changes of generalized displacement variables such as volume, strain, magnetization, polarization, etc. The natural way to induce changes of these variables is by means of the application or removal of their corresponding conjugated generalized forces (or fields). For instance, the fields conjugated to volume, strain, magnetization and polarization are respectively pressure, stress, magnetic field and electric field. Actually, changes of these fields will give rise to barocaloric, elastocaloric, magnetocaloric and electrocaloric effects, respectively. Caloric effects are especially interesting in the case of so-called multiferroic materials which display cross-variable response. In this case, a given generalized displacement can be modified by more than one field. This is a consequence of the interplay between the different generalized variables in the system. Indeed, this is, for instance, the case of magnetic shape-memory materials, the class of systems of interest here, which show strong coupling between magnetic and mechanical variables.

Thermodynamics provides a very convenient framework enabling us to establish a unified treatment at a macroscopic scale of caloric effects, regardless of the actual complexity of the particular system of interest. From this viewpoint, we consider a generic closed system[3] described by n relevant generalized displacements $\{\mathbf{X}_i\}$ $(i = 1, \ldots, n)$. The internal energy is a function

$$U = U(S, \{\mathbf{X}_i\}) \tag{1}$$

[3] Since we only consider closed systems, the number of atoms of the constituents of the studied system are fixed.

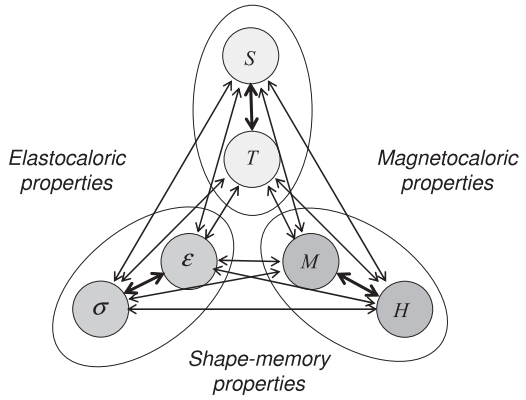

Figure 1. Thermodynamic relations between thermal, elastic and magnetic variables. Magnetic shape-memory properties arise from the cross magnetic–elastic variable response. Magnetocaloric and elastocaloric properties arise, respectively, from the interplay between thermal and magnetic and thermal and elastic variables. Variables connected by thick lines are conjugated in the thermodynamic sense (same tensorial rank).

with $n + 1$ independent variables, where S is the entropy. The generalized forces $\{\mathbf{x}_i\}$ $(i = 1, \ldots, n)$ thermodynamically conjugated to the generalized displacements are given by

$$\mathbf{x}_i = \left(\frac{\partial U}{\partial \mathbf{X}_i}\right)_{S,\mathbf{X}_{j\neq i}}. \tag{2}$$

The temperature is defined as $T = (\partial U/\partial S)_{\{\mathbf{X}_i\}}$ and plays the role of the conjugated variable to the entropy. Indeed, each pair of conjugated variables have the same tensorial order so that the tensorial product $\mathbf{x}_i \cdot \mathrm{d}\mathbf{X}_i$ is a scalar that quantifies the (reversible) work associated with differential changes of the generalized displacement induced by the corresponding generalized force. The existence of interplay between different degrees of freedom must be taken into account through the explicit dependence of each coordinate $\mathbf{X}_i$ on the remaining variables $\{\mathbf{X}_{j\neq i}\}$. On the other hand, caloric effects result from the explicit dependence of $\{\mathbf{X}_i\}$ on the entropy (and, implicitly, on its conjugated coordinate, the temperature). For our present interest, we need to consider, in addition to thermal coordinates, magnetic and mechanical variables. Thus, the relevant pairs of conjugated variables are magnetic-field/magnetization and stress/strain. The thermodynamics in these class of systems is schematically represented in figure 1. Magnetic shape-memory effects are related to the interplay between magnetic and mechanical variables, while the elastocaloric and magnetocaloric effects originate, respectively, from the dependence of the mechanical and magnetic variables on the thermal variable (entropy and temperature).

In order to quantify caloric effects, it is convenient to express differential changes of entropy in terms of differential changes of fields and temperature, taken as independent variables. The corresponding expression is

$$\mathrm{d}S = \frac{C}{T}\,\mathrm{d}T + \sum_{i=1}^{n}\left(\frac{\partial \mathbf{X}_i}{\partial T}\right)_{\{\mathbf{x}_{j=1,\ldots,n}\}} \cdot \mathrm{d}\mathbf{x}_i, \tag{3}$$

where the definition of the heat capacity C at constant values of the fields, $(\partial S/\partial T)_{\{\mathbf{x}_{j=1,\ldots,n}\}} = C/T$, has been taken into account in the first term on the right-hand side of equation (3). The generalized Maxwell relations:

$$\left(\frac{\partial S}{\partial \mathbf{x}_i}\right)_{T,\mathbf{x}_j\neq i} = \left(\frac{\partial \mathbf{X}_i}{\partial T}\right)_{\mathbf{x}_{j=1,\ldots,n}} \tag{4}$$

have been used to express the second term. From equation (3), the reversible entropy change induced by an isothermal change of a given field $\mathbf{x}_i$ (from 0 to a value $\mathbf{x}_i$) is obtained as

$$\Delta S(0 \to \mathbf{x}_i) = \int_0^{\mathbf{x}_i} \boldsymbol{\xi}_i \cdot \mathrm{d}\mathbf{x}_i, \tag{5}$$

where $\boldsymbol{\xi}_i = (\partial \mathbf{X}_i/\partial T)_{\mathbf{x}_j=1,\ldots,n}$. The corresponding adiabatic change of temperature is given by

$$\Delta T(0 \to \mathbf{x}_i) = -\int_0^{\mathbf{x}_i} \frac{T}{C}\,\boldsymbol{\xi}_i \cdot \mathrm{d}\mathbf{x}_i. \tag{6}$$

From these equations, it is clear that the caloric effect associated with the i coordinate is controlled by the response function $\boldsymbol{\xi}_i$ which quantifies the entropy change resulting from the ordering/disordering effects associated with all degrees of freedom induced by the application of the field $\mathbf{x}_i$. Adiabatically, this ordering/disordering effect is 'absorbed' by the lattice (taken into account through its heat capacity C), thus giving rise to a temperature change. For the particular case of the magnetocaloric effect, the relevant response function is $\xi_M = (\partial M/\partial T)_{H,\ldots}$, where M is the component of the magnetization in the direction of the applied field $\mu_0 H$ (μ_0 is the magnetic permeability of free space). Thus, the field-induced isothermal entropy and adiabatic temperature changes are given by the expressions

$$\Delta S(0 \to H) = S(T, H) - S(T, 0) = \mu_0 \int_0^H \xi_M\,\mathrm{d}H, \tag{7}$$

and

$$\Delta T(0 \to H) = T(S, H) - T(S, 0) = -\mu_0 \int_0^H \frac{T\xi_M}{C}\,\mathrm{d}H. \tag{8}$$

It is interesting to point out that while in general the response function ξ_M is negative, a positive value is not forbidden by thermodynamics. In those regions of the space of thermodynamic variables where this occurs, a magnetic field will cause an increase of entropy when applied isothermally and a decrease of temperature (cooling) when applied adiabatically. Such a non-conventional magnetocaloric effect is denoted as the inverse magnetocaloric effect. As will be discussed later, inverse effects often occur in the vicinity of phase transitions as a consequence of the strong interplay between magnetism and other degrees of freedom.

Other caloric effects of interest are the electrocaloric, barocaloric and elastocaloric effects. The relevant response functions are $\xi_P = (\partial P/\partial T)_{E,\ldots}$, where P is the polarization component in the direction of the applied electrical field E in the case of the electrocaloric effect, $\xi_V = (\partial V/\partial T)_{p,\ldots}$ (V is volume and p is pressure) for the barocaloric effect

and $\xi_\varepsilon = (\partial\varepsilon/\partial T)_{\sigma,\ldots}$ (σ is an uniaxial stress and ε the corresponding strain) in the case of the elastocaloric effect. Notice that the barocaloric effect is the basis of the traditional vapour-compression cooling technology. On the other hand, the electrocaloric effect has been largely ignored since only small effects were expected. Very recently, however, giant electrocaloric effects have been reported in $PbZr_{0.95}Ti_{0.05}O_3$ films near the ferroelectric Curie point which have prompted interest in this phenomenon [17]. Also, large elastocaloric effects induced by the application of uniaxial stress have been reported in a number of intermetallic and rare-earth compounds in the vicinity of magnetostructural [15, 18] and purely structural [19] phase transitions. In general, giant caloric effects are expected to occur in the vicinity of phase transitions where the response functions ξ_i are expected to be large. Section 2.1 will be devoted to the study of the magnetocaloric effect in the region of phase transitions.

2.1. Magnetocaloric effect in the vicinity of phase transitions

Magnetic phase transitions are found more commonly to be of a continuous nature. In systems showing this class of continuous transitions, large magnetocaloric effects are expected around the Curie point where ξ_M is large. This is, for instance, the case of Gd which orders magnetically near room temperature and is a conventional ferromagnet, and is still the prototype material for room temperature magnetic cooling applications [20]. The common continuous character of these transitions is related to the invariance under inversion of magnetization (due to time-reversal symmetry) which compels the free energy to contain only even powers in the magnetization. This is, however, not a sufficient condition and first-order magnetic transitions are possible due, for instance, to interaction of the magnetic degrees of freedom and a secondary field [21, 22]. Typically, the secondary field is related to lattice displacements due to different sorts of interplay of the magnetic degrees of freedom with the crystal lattice. An example of interplay is the exchange magnetostrictive mechanism proposed by Bean and Rodbell [23]. These class of transitions will be denoted here as magnetostructural transitions. Interestingly, these transitions usually involve a strong entropy content and can be field-induced. Therefore, materials undergoing these kinds of transitions are very attractive for applications based on magnetocaloric properties since giant effects are expected in their vicinity.

We will not discuss here the magnetocaloric effect associated with continuous phase transitions. This problem has been discussed, for instance, in [24]. Here, we will focus on magnetostructural phase transitions which involve both changes of magnetic and structural properties. With the aim of studying magnetocaloric effects associated with these first-order transitions, we assume that the dependence of the magnetization in the vicinity of the transition is of the general type:

$$M(H,T) = M_0 + \Delta M(H)\mathcal{F}\left[\frac{T - T_t(H)}{\Delta T(H)}\right]. \tag{9}$$

In the preceding expression of the magnetization, M_0 is assumed to be constant (independent of temperature and magnetic field), which supposes that any temperature or field dependence of the magnetization from outside the transition region has been subtracted. This means that we will not take the contribution to the magnetocaloric effect from outside the transition region into consideration. ΔM is the magnetization change defined as the difference between the magnetizations of the low-and high-temperature phases. $\mathcal{F}$ is an arbitrary continuous function (not necessarily analytic) which varies from 0 to 1 within the range $\Delta T(H)$. In general, first-order phase transitions show hysteresis, and thus this range is different for the forward transition on cooling and for the reverse transition on heating. T_t is an estimate of the corresponding transition temperature[4]. For an ideal first-order transition taking place in strict equilibrium, no hysteresis occurs and $\Delta T \to 0$. Therefore

$$\lim_{\Delta T\to 0} \mathcal{F} = h(T - T_t), \tag{10}$$

where h is a Heaviside step function (which describes the discontinuity in the magnetization). Assuming that ΔM is independent of H, the following expression is then easily obtained from equation (7):

$$\Delta S = \begin{cases} -\dfrac{\mu_0 \Delta M}{|\alpha|} & \text{for } T \in [T_t(0), T_t(H)] \\ 0 & \text{for } T \notin [T_t(0), T_t(H)], \end{cases} \tag{11}$$

where $\alpha \equiv \mathrm{d}T_t/\mathrm{d}H$. This derivative is related to the discontinuities in the magnetization and entropy through the Clausius–Clapeyron equation[5]

$$\frac{\mathrm{d}T_t}{\mathrm{d}H} = -\mu_0 \frac{\Delta M}{\Delta S_t}. \tag{12}$$

Thus, we conclude that, in this case, the field-induced entropy change coincides with the transition entropy change ΔS_t. Note that $T_t(H) - T_t(0)[=\Delta T_t = -\mu_0(\Delta M/\Delta S_t)H]$ is the shift of the transition temperature induced by the field H. Interestingly, when $\Delta M > 0$ ($\alpha > 0$), the magnetocaloric effect is conventional, while it is inverse when $\Delta M < 0$ ($\alpha < 0$). This last situation can occur, for instance, when the magnetization of the low-temperature phase is lower than the magnetization of the high-temperature phase (see figure 2).

In this ideal case, the adiabatic field-induced temperature change is determined from the Clausius–Clapeyron equation. The maximum change of temperature can be obtained as $\Delta T_{max} \simeq T\Delta S_t/C$. This expression, which is adequate at high temperatures when relative temperature changes are small

[4] Often, in experiments, T_t is taken from the estimation of the inflection point of the magnetization curve.

[5] There has been a lot of controversy on whether or not expression (7) based on Maxwell relations can be used in the case of first-order phase transitions. See, for instance, the paper by Giguère *et al* [25] and comments with corresponding replies to this paper by Gschneider *et al*, Sun *et al* and Földeàki *et al* [25]. Actually the derivation proposed here clarifies this point by showing that equation (7) is of general use and that it yields Clausius–Clapeyron when the change of magnetization occurs through a discontinuity.

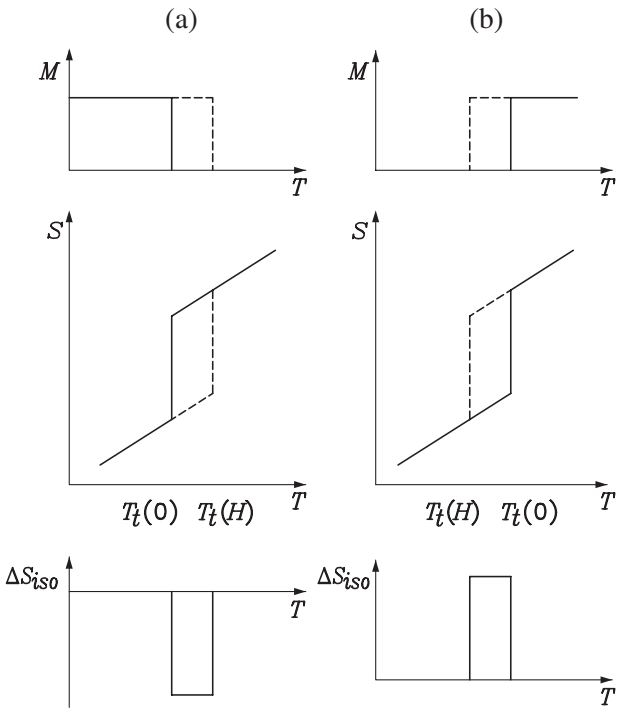

Figure 2. Schematic representation of the magnetization, entropy and field-induced entropy change in the vicinity of a first-order metamagnetic transition. In the M versus T and S versus T figures, continuous lines indicate the zero-field behaviour, while discontinuous lines correspond to an applied field H. The slope of the curves S versus T is C/T (in the figure C is assumed to be independent of H). (a) The field shifts the transition to a higher temperature. This corresponds to $\Delta M > 0$. In this case the magnetocaloric effect is conventional. (b) The field shifts the transition to a lower temperature. In this case $\Delta M < 0$ and the inverse magnetocaloric effect occurs.

enough, assumes that the heat capacity does not depend on the magnetic field[6].

In real materials, magnetostructural transitions usually spread over a certain range of temperatures. There are several factors that can explain this fact including the existence of composition gradients, defects, etc. In the case of transitions that involve strain, such as those of interest in this review, such a temperature spread is essentially a consequence of the fact that elastic strain is induced by the crystal lattice misfit between product and parent phases. When the elastic energy can balance (or even exceed) the transition driving force provided by the difference of chemical free energies of both phases, a thermoelastic equilibrium is possible [26]. In this case, the transition can only take place through an optimum transition path. Along this path, almost complete accommodation of the transformation-induced elastic strain is achieved. Therefore, when cooling from the high-temperature phase, the transition starts at a given temperature, and the system needs to be continuously cooled down to make the transformed fraction of the new phase to increase. Indeed, this behaviour is favoured by the fact that thermal fluctuations play a minor role [27]. Actually, accurate observations reveal that these transitions proceed through a series of discrete jumps connecting metastable states in which the thermoelastic equilibrium condition is satisfied [28]. Typically, these jumps occur in time intervals much smaller than the time of appreciable variation of the driving force. Thus, the system spends the overwhelming majority of time in a situation of thermoelastic equilibrium.

In the general case of transitions spreading over a temperature interval, it is convenient to define an average field-induced entropy change for each (maximum) applied field H as

$$\langle \Delta S(H) \rangle = \frac{1}{\overline{|\Delta T(H)|}} \int_{\Delta T} \Delta S(T, H)\, \mathrm{d}T, \qquad (13)$$

where $\overline{|\Delta T(H)|}$ is an effective temperature range which takes into account the shift of the transition induced by the magnetic field. The following expression can then be obtained:

$$\langle \Delta S(H) \rangle = -\frac{\mu_0}{\overline{|\Delta T(H)|}} \int_0^H \Delta M(H)\, \mathrm{d}H. \qquad (14)$$

This expression indicates that in the vicinity of a magnetostructural transition, the magnetocaloric effect is essentially controlled by the behaviour of the change of magnetization at the transition (in the ideal case $\langle \Delta S(H) \rangle = \Delta S_t$).

It is interesting to note that integrating the Clausius–Clapeyron equation (equation (12)), while assuming that ΔS_t is independent of the applied field, gives

$$\Delta T_t(H) = \frac{\mu_0}{|\Delta S_t|} \int_0^H \Delta M(H)\, \mathrm{d}H, \qquad (15)$$

which from comparison with equation (14) shows that even for non-ideal first-order transitions, the behaviour of the average field-induced entropy change and the corresponding change of transition temperature are expected to follow a comparable qualitative dependence as a function of applied field.

2.2. Non-equilibrium effects

So far, we have analysed the magnetocaloric effect within the framework of equilibrium thermodynamics. We have already mentioned that first-order transitions commonly occur with hysteresis which is a signature of non-equilibrium effects. In most magnetostructural transitions, and especially in those which take place in Heusler shape-memory alloys, deviations from equilibrium are small [12]. It is, however, important briefly to analyse the consequences of the fact that these transitions do not occur in strict equilibrium. For this, our starting point will be the Clausius inequality:

$$\oint \frac{\delta q}{T} \leqslant 0, \qquad (16)$$

where q is the heat involved in a given process. Notice that the equality holds for equilibrium. Introducing reversible and irreversible entropy contributions, the previous inequality can be expressed in local form as

$$\mathrm{d}S = \frac{\delta q}{T} + \delta S_i, \qquad (17)$$

[6] Notice that the field necessary to reach this maximum change of temperature is a field that enables us to adiabatically span the whole transition. Indeed, this field depends on the heat capacity of the system (see figure 2).

where $\delta S_i \geqslant 0$ is the entropy production term. By substituting the differential entropy change $\mathrm{d}S$ in expression (3) by (17), it is possible to obtain the following inequalities which are to be satisfied by the isothermal entropy change and the adiabatic temperature change induced by a change of the field from 0 to H given as

$$\Delta S(0 \to H) \geqslant \int_0^H \frac{\delta q}{T}, \tag{18}$$

and

$$\Delta T^{\mathrm{irr}}(0 \to H) \geqslant \Delta T(0 \to H). \tag{19}$$

From the second of these equations, it is clear that the cooling efficiency through adiabatic demagnetization ($\xi < 0$) decreases due to non-equilibrium effects, as expected.

In the case of a magnetostructural phase transition, the dissipated energy can be estimated as $E_{\mathrm{diss}} = TS_i = \mu_0(H - H_0)\Delta M$, where H_0 is the equilibrium transition field at temperature T and H is the actual transition field at this temperature. ΔM is the magnetization discontinuity. It is straightforward to show that when dissipation is taken into account within the above framework, the Clausius–Clapeyron equation is modified and takes the following form:

$$\mu_0 \frac{\mathrm{d}H}{\mathrm{d}T} = -\frac{\Delta S}{\Delta M} + \frac{1}{\Delta M}\frac{\mathrm{d}E_{\mathrm{diss}}}{\mathrm{d}T}, \tag{20}$$

which assumes that ΔM is constant. Notice that E_{diss} is usually weakly dependent on temperature, and thus the last term in the previous equation is small which shows that the Clausius–Clapeyron equation is still a good approximation.

2.3. Experimental determination of magnetocaloric effects

Experimental determination of the isothermal field-induced entropy change is usually based on equation (7). This is an indirect determination which relies on the measurement of M versus H with close-enough temperature intervals[7]. The entropy change is then obtained as [29]

$$\Delta S[0 \to H; T(k)] = \mu_0 \frac{1}{\Delta T_k}\left[\int_0^H M(T_{k+1})\,\mathrm{d}H - \int_0^H M(T_k)\,\mathrm{d}H\right], \tag{21}$$

where $T(k) = (T_{k+1} + T_k)/2$, $\Delta T_k = T_{k+1} - T_k$ and the integrals are computed numerically. When the previous expression is used to compute the field-induced entropy change in the vicinity of a magnetostructural transition, the obtained result includes the contribution from a possible field and temperature dependence of the magnetization outside the transition. For high-enough fields, this contribution can yield a field-induced entropy change larger than the transition entropy change. From proper estimation and subtraction of this contribution to the whole field-induced entropy change, it has been shown that for fields large enough to complete the transition, the remaining contribution corresponds to the transition entropy change obtained, for instance, by using the Clausius–Clapeyron equation [30].

The field-induced entropy change can also be obtained from measurements of the heat capacity at selected values of the magnetic field (see [29, 31]) from which the entropy can be computed as

$$S(T, H) = \int_0^T \frac{C(T, H)}{T}\,\mathrm{d}T. \tag{22}$$

Then, the entropy change at temperature T associated with a change of field $0 \to H$ is estimated as

$$\Delta S(0 \to H; T) = S(T, H) - S(T, 0). \tag{23}$$

Heat flux scanning calorimetry provides a method suitable for direct determination of $\Delta S(0 \to H)$ [32–36]. These calorimeters are well adapted to study magnetocaloric effects associated with magnetostructural first-order transitions. In this case, calorimetric peaks (thermal power $\dot{q}$ versus time) can be obtained by sweeping the magnetic field and keeping the temperature constant. From integration of the calorimetric signal, $q(0 \to H)/T$ can be obtained which, as shown in section 2.2, could differ from $\Delta S(0 \to H)$ if the studied process occurs out of equilibrium. When dissipative effects are weak, as is the case in magnetostructural transitions considered here, q/T represents a good estimation of field-induced entropy change (see, for instance, [37]).

The adiabatic field-induced temperature change is usually determined from direct thermometric measurements. This requires using large-enough samples in order to avoid the influence of the thermometer. Adiabaticity is ensured by suitable isolation of the sample from the external environment and a fast-enough application of the field. The adiabatic change of temperature is then estimated as the difference between sample temperatures obtained before and after applying the field (see, for instance, [38]). This change of temperature can also be computed from magnetization curves using equation (8). In this case, measurements of heat capacity are also needed. If the heat capacity shows little dependence on the magnetic field and temperature changes are small, $\Delta T(0 \to H)$ can be estimated to a good approximation as

$$\Delta T(0 \to H) = -\frac{T}{C}\Delta S(0 \to H). \tag{24}$$

According to equation (19), discrepancies between direct and indirect determinations of $\Delta T(0 \to H)$ should be related to non-equilibrium effects. A quantitative estimation of dissipative effects on magnetocaloric properties in the vicinity of first-order and continuous transitions based on comparison of direct and indirect measurements of adiabatic temperature changes has been shown [39] to provide very good results.

Another interesting method is based on the comparison of a set of isothermal magnetization curves and an adiabatic magnetization curve. The adiabaticity is approached by applying a short-enough magnetic field pulse. The crossing points of the adiabatic curve with the set of isothermal curves determine the fields at which the studied specimen has a given temperature. Therefore, at each field the adiabatic field-induced temperature change can be obtained [40].

[7] When the entropy change corresponds to a field change from $0 \to H$, care must be taken that for all isotherms the initial state at $H = 0$ is a demagnetized state.

3. Phase stability: structure and magnetism

The occurrence of magnetic-field-induced structural transitions, as introduced in section 2.1, is an indication of the presence of an intimate relationship between structural and magnetic degrees of freedom at the microscopic level. It is necessary to understand this relationship in order to be able to gain an insight into the details of the martensitic transformation and, thereby, into the microscopic principles governing magnetocaloric and magnetic shape-memory effects. In the following, we provide some background concerning the structures in the austenitic and martensitic states of Heusler-based systems. We then provide details on the relationship between structural and magnetic properties.

3.1. Structure and magnetism of Ni–Mn-based martensitic Heusler alloys

3.1.1. The structures. In the austenite state, Heusler alloys have an $L2_1$ structure (space group $Fm\bar{3}m$) which consists of four interpenetrating fcc sublattices, as shown in figure 3(a). For the stoichiometric composition, Ni atoms occupy the 8c positions (in Wyckoff notation), while Mn and Z atoms occupy 4a and 4b positions, respectively [41]. When the temperature is decreased, they can undergo a martensitic transformation and acquire a number of structures. In particular, Ni–Mn–Z Heusler alloys (Z: Ga, Al, In, Sn, Sb) transform to the $L1_0$ tetragonal structure at low Z concentrations, since this is also the ground-state structure of the parent compound $Ni_{50}Mn_{50}$. The relationship between the $L2_1$ and the tetragonal structures is given in figure 3(a) and the tetragonal structure is also shown separately in figure 3(b). This is not the only structure reported in the martensitic state, and modulated structures related to the tetragonal structure can be found especially at higher Z concentrations. The most common are the 5M and the 7M modulated structures. The tetragonal structure viewed from the top plane in figure 3(b) is shown in figure 3(c). From this perspective, the generated modulations can be seen for the 5M and 7M cases in figures 3(d) and 3(e). 'M' refers to the monoclinicity resulting from the distortion associated with the modulation. The 5M and 7M modulations are sometimes referred to as 10M and 14M.

Ni_2MnGa is the only Ni–Mn-based Heusler alloy with the exact 2–1–1 stoichiometry that undergoes a martensitic transformation and almost no volume change occurs across the transition [9, 42]. Therefore, it is relatively easy to visualize the structures shown in figure 3 for Ni_2MnGa. Similar structures are also encountered in other Ni–Mn–Z Heusler alloys undergoing martensitic transformations [43, 44]. The differences are that in these alloys, the transformation takes place at off-stoichiometric compositions, depending on what the Z species is, and volume changes occur across the martensitic transition [45]. These introduce complexities in depicting the crystallographic relationships between the austenitic and martensitic states which is principally straightforward for Ni_2MnGa. Nevertheless, the observation of similar modulated states in alloys with and without Ga is an indication that the martensitic transformation in alloys having a Z species other than Ga can be described by similar crystallographic relationships.

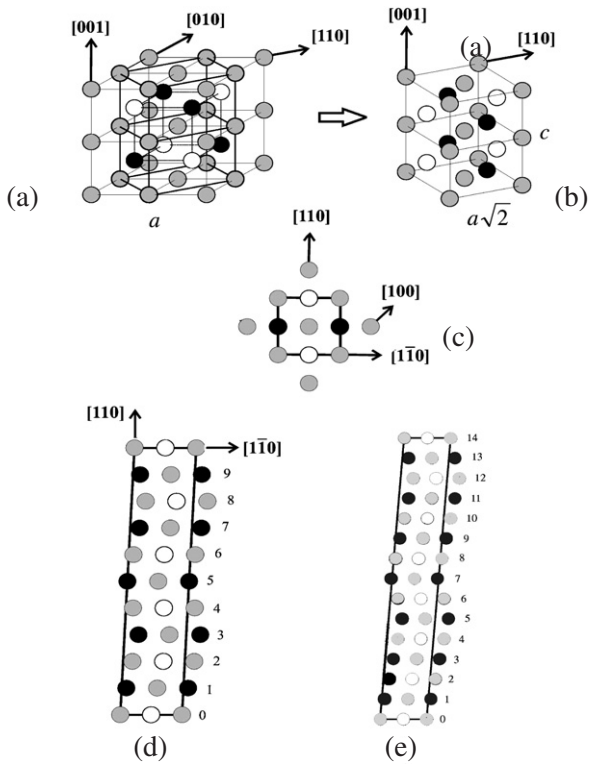

Figure 3. Austenite and martensite structures of Heusler alloys shown for the case of Ni_2MnGa. Light grey: Ni, white: Mn, black: Ga. (a) The $L2_1$ Heusler structure showing also the relationship with the tetragonal unit cell, which is also shown in part (b). (c) The tetragonal unit cell viewed from the top and (d) the 5 M (or 10 M) and (e) 7 M (or 14 M) modulated structures obtained by shearing the tetragonal cell.

Which of the structures stabilize in the martensitic phase of Ni–Mn–Z alloys depends on the composition. Figure 4 shows the magnetic and structural phase transition temperatures of Ni–Mn–Z Heusler alloys with Z as Sn, In and Ga plotted as a function of the valence electron concentration per atom e/a. The composition in at.% is given in the upper axis. e/a is calculated as the concentration-weighted average of the valence electrons. In the case of Heusler alloys, these are the s, p and d electrons of the constituents. The ferromagnetic (FM) Curie temperatures of the austenitic and martensitic states are given as T_C^A and T_C^M, respectively, and the martensite 'start' temperature is given as M_s. One sees in this figure that in all three cases the ground-state structure evolves essentially as cubic $\rightarrow$ 10 M $\rightarrow$ 14 M $\rightarrow$ $L1_0$ with increasing e/a. The width of the compositional regions depends on the Z species. The data for Z as Sn and In are for alloys with a constant Ni composition of 50 at.% [43, 44, 46, 47], whereas those for Ni–Mn–Ga are collected from various sources and there are no constraints on the composition of any of the elements, hence the increased scattering in the data [48]. Further details of magnetic and structural transition properties are discussed in relation to figure 6 under section 3.2.1.

We point out here that the structures presented above are not the only modulated structures encountered in these

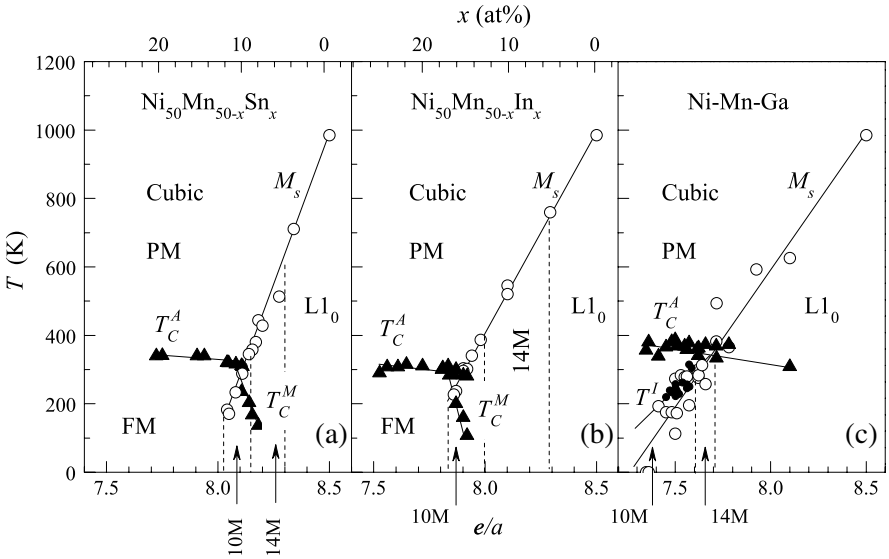

Figure 4. The magnetic and structural phase diagram of Ni–Mn–Z Heusler alloys with Z as (a) Sn, (b) In and (c) Ga. The triangles and the circles correspond to the magnetic and martensitic transformation temperatures respectively. The regions corresponding to the different structures are separated by discontinuous lines. Small solid circles in (c) correspond to the premartensitic transition temperature.

alloys, and there are claims that other modulated structures can better describe the data, particularly in the bordering regions of the phases as shown in figure 4. Much work is currently being carried out to resolve many details of diffraction spectra [42, 49, 50].

3.1.2. Magnetic properties. Ni–Mn-based martensitic Heusler alloys show a number of features in the temperature dependence of the magnetization $M(T)$ depending on how the measurement is carried out. Figure 5 shows $M(T)$ for Ni–Mn–Z alloys. When measured in a small external field of 50 Oe, the $M(T)$-data for Ni–Mn–Z alloys that undergo a martensitic transformation at a temperature below T_C^A are similar[8]. Only Ni–Mn–Ga shows some differences. Otherwise, a representative plot of $M(T)$ of all such samples is summarized with the data for $Ni_{50}Mn_{34}In_{16}$ in figure 5(a) [44]. The data are taken on a zero-field-cooled (ZFC), field-cooled (FC) and field-heating (FH) sequence. Following the FC data from the high-temperature paramagnetic end, $M(T)$ shows a fast increase with decreasing temperature at T_C^A as the FM state sets in. As the temperature further decreases, the martensitic transformation begins at M_s, below which $M(T)$ decreases until the temperature reaches a value corresponding to the local minimum. This temperature is designated as the martensite finish temperature M_f. At a lower temperature, $M(T)$ resumes to increase with decreasing temperature as FM ordering in the martensitic state occurs at T_C^M. In a manner similar to the forward austenite-to-martensite transition, the reverse transformation occurring on heating starts at the austenite start temperature A_s and finishes at the austenite finish temperature A_f, as can be found both in the curves corresponding to the ZFC and FH states. The splitting between the ZFC state and the FC or the FH state is mainly due to the anisotropy of the FM state below T_C^M, but it can also be partially related to the presence of antiferromagnetic (AF) components that pin the FM matrix in different spin configurations, depending whether a cooling field is present or absent.

The situation for Ni–Mn–Ga is not too different, although $M(T)$ runs rather flat below M_s, as shown for an $Ni_{50}Mn_{27}Ga_{23}$ sample in figure 5(b). This is due to the fact that both the twin boundary mobility is higher and the magnetocrystalline anisotropy is stronger in the martensitic state of Ni–Mn–Ga. Even in such small magnetic fields, the external magnetic field is capable of partially aligning the variants along their easy axis so that the ZFC–$M(T)$ attains finite values already at low temperatures.

The drop in $M(T)$ below M_s is a feature that is found in all Ni–Mn–Z alloys when measured in low external fields and is related to an initial loss of FM ordering (see section 3.3). When $M(T)$ is measured in high fields, as shown in figure 5(c), this feature does not vanish, instead it remains pronounced except in the case of Z as Ga, where now a slight increase in $M(T)$ around M_s is found on decreasing temperature. In all the other alloys, the magnetization in the martensitic state is lower than the magnetization in the austenitic state.

3.2. Properties of martensitic Heuslers in relation to the valence electron concentration

A useful experimental guide to extract information on the general properties of magnetostructural transitions in relation to electronic properties is to examine the measured parameters such as volume, magnetic moment, transition temperatures, etc, as a function of e/a. Observed systematic changes in these parameters with respect to e/a can provide a useful guide for tailoring materials to a particular interest [52, 53].

[8] The magnetic behaviour of Ni–Mn–Al alloys does not conform to the general trends exhibited by all other alloys in the Ni–Mn–Z family. The main reason for such a different behaviour is the fact that, owing to kinetic reasons, it does not achieve a long-range $L2_1$ order but it exhibits B2 order instead, for which the magnetic exchange is predominantly antiferromagnetic. See, for instance, Acet *et al* [51].

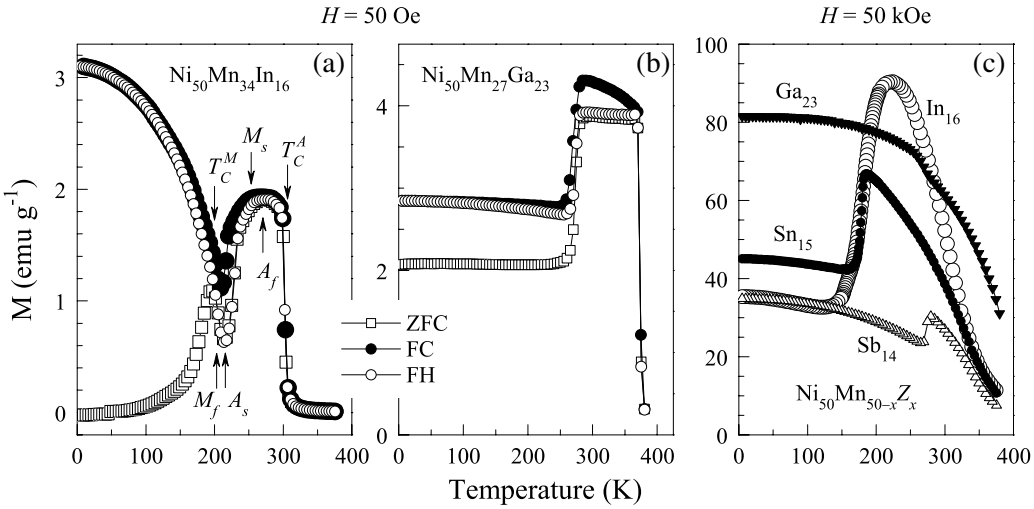

Figure 5. $M(T)$ for Ni–Mn–Z Heusler alloys. (a) A typical low-field measurement ($H = 50$ Oe) represented by the data for Z as In. (b) A typical low-field measurement ($H = 50$ Oe) for Ni–Mn–Ga. (c) High-field $H = 50$ kOe $M(T)$ measurements for Z as Ga, In, Sn and Sb.

3.2.1. Structural and magnetic transformation temperatures. The phase diagrams for Ni–Mn–Z were plotted for each Z species in figure 4 to show the evolution of the various structures with composition. To be able to compare in more detail the magnetic and structural transition temperatures of these systems we collect the phase diagram in a single plot in figure 6. The starting composition common to all alloys is $Ni_{50}Mn_{50}$ with $e/a = 8.5$, which is in the tetragonal $L1_0$ state already at high temperatures. Adding the third element Z progressively decreases e/a, and along with it M_s also decreases. However, what one furthermore observes is that the slope of the curves are different for different Z species. For practical purposes, we find that the slopes are large in all cases with about 80 K per 0.1 e/a for Z as Ga and nearly 270 K per 0.1 e/a for Z as Sb. 0.1 e/a corresponds to a small compositional variation of about 5 and 2 at.% for Z as Ga and Z as Sb, respectively. Although the general tendency that M_s increases with increasing e/a in a similar manner for all Z species is understood from the figure, more precise information should be able to be obtained when other parameters—such as the atomic volume being an important one—could also be taken into account. Another important point is that each of the Z species have different crystallographic structures in elemental form. Therefore, when alloyed to Ni–Mn, it can be expected that the composition dependence of the binding forces develop differently for each Z species, so that the evolution of the electronic structure with composition is also different. This could also influence the e/a dependence of the structural and magnetic transition temperatures, and therefore such considerations have to be taken into account to improve our understanding of the observed properties of martensitic Heusler alloys.

Whereas M_s changes rapidly with e/a, T_C^A for each series with a particular Z species shows little variation, although there is a tendency for T_C^A to decrease with increasing e/a. This is related to the weakening of ferromagnetic coupling with increasing Mn content as the probability of Mn having another Mn atom as nearest neighbour increases. Decreasing Mn–Mn distances or increasing number of Mn–Mn nearest neighbours strengthens antiferromagnetic (AF) exchange, leading to an eventual drop in T_C. T_C^A also lies generally higher when Z ranges from In to Sb in the case when the Ni concentration is held at 50 at.%. This depends on how each Z species influences the ferromagnetic exchange.

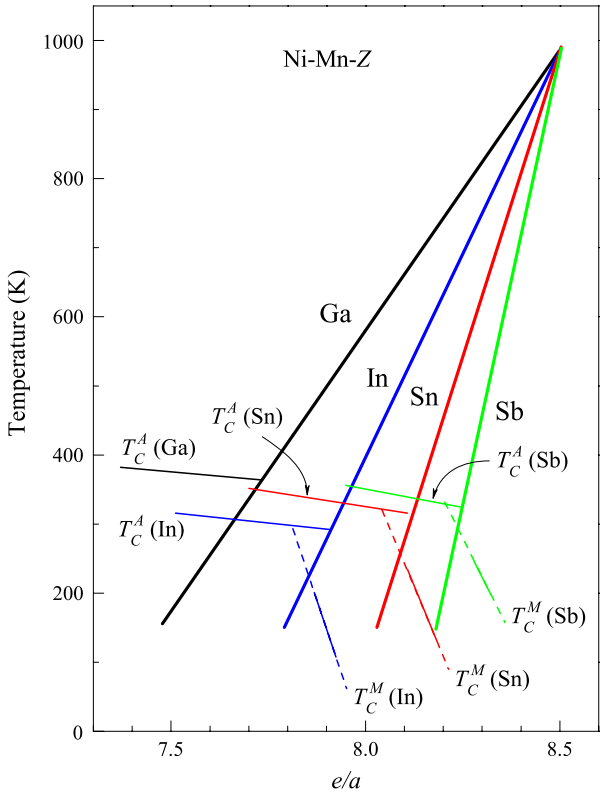

Figure 6. The e/a dependence of the martensitic transition temperature (M_s) and the Curie temperature in austenitic (T_C^A) and martensitic (T_C^M) states for Ni–Mn–Z Heusler alloys with Z as Ga, In, Sn and Sb.

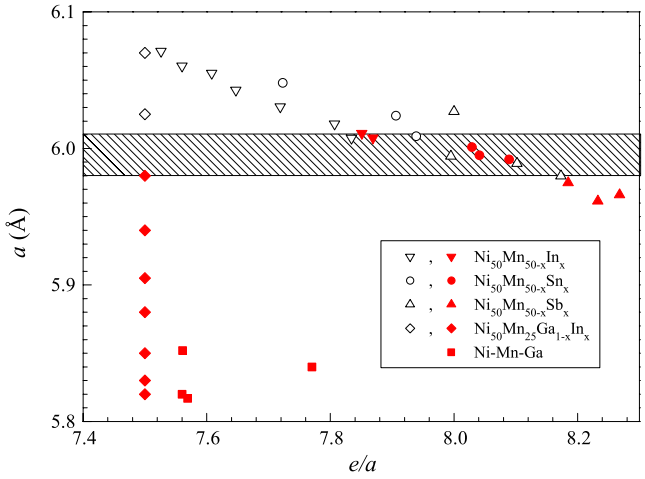

Figure 7. The e/a dependence of the lattice parameter of the cubic phase at room temperature in Ni–Mn-based Heusler alloys. The lattice parameters for Ni–Mn–In–Ga, where In and Ga are isoelectronic, are also shown. Alloys undergoing martensitic transformations are shown with filled symbols. Those that are stable are shown with open symbols. Samples above the shaded region do not transform martensitically.

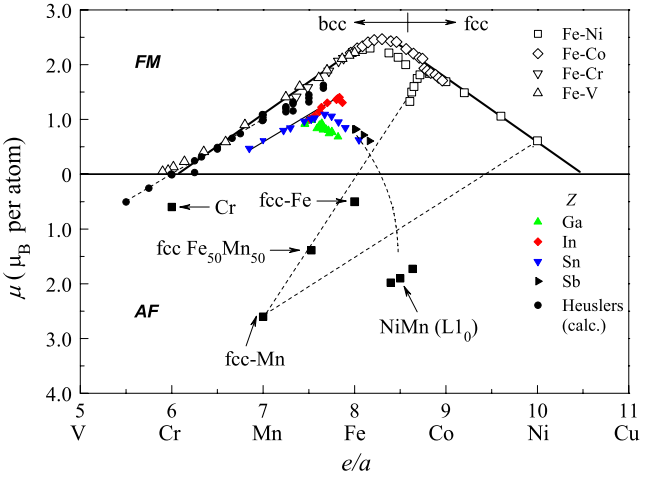

Figure 8. The e/a dependence of the magnetic moment for 3d and Heusler alloys. The filled circles are calculated values and the open symbols represent the moments of 3d metals and alloys. Filled small symbols represent the moments of Ni–Mn–Z Heuslers and filled squares represent those of antiferromagnets.

Rather different from the behaviour of T_C^A, T_C^M drops rapidly with increasing e/a (except for Z as Ga), e.g. for Z as In, T_C^M is expected to vanish around $e/a = 8.0$. The question is then whether antiferromagnetism would appear at $e/a > 8.0$. The structure of these alloys in their martensitic states are either $L1_0$ (or a modulated structure derived from $L1_0$) and the structure of the parent composition $Ni_{50}Mn_{50}$ is also $L1_0$. Since $Ni_{50}Mn_{50}$ is AF with a Néel temperature T_N of about 1200 K, a rapid strengthening of AF exchange should occur at $e/a > 8.0$ where long-range ferromagnetic exchange essentially vanishes. Indeed AF exchange is found to occur for $e/a > 8.0$ [43, 44], although, presently, measurements have not been carried out to high-enough temperatures allowing T_N to be determined.

3.2.2. The lattice parameters in the $L2_1$ state. Figure 7 shows the e/a dependence of the lattice constants at room temperature in the $L2_1$ phase for Ni–Mn–Z [54]. The data shown with filled symbols represent alloys that undergo a martensitic transformation. Those shown with open symbols are stable in the $L2_1$ phase. One observes that a martensitic transformation occurs in alloys having a critical value of the lattice constant $a_c \approx 6$ Å or less in the austenitic state. Since In and Ga are isoelectronic, replacing one of these elements by the other causes a change in the lattice constant without altering the electron concentration. Therefore, for the series $Ni_{50}Mn_{25}Ga_{25-x}In_x$, a increases on replacing Ga with In, and one finds a crossover in the stability as a runs through the critical value. This shows that the atomic volume is a parameter that by all means has to be taken into account in order to be able to fully understand the electronic properties of these alloys.

3.2.3. The electron concentration dependence of the magnetic moment. A plot of the e/a dependence of the magnetic moment can provide useful systematics concerning the electronic properties of metallic materials. Figure 8 shows the Slater–Pauling (SP) curve—the e/a dependence of the magnetic moment per atom μ—in a modified form where additionally moments for some AF systems are also included. The open symbols in the upper portion of the curve represent the magnetic moment of FM 3d alloys. For these alloys, the fcc state is stable to e/a values corresponding to somewhat above the maximum in the curve at $e/a \approx 8.5$. Below this value the bcc state is stable. Deviations from the SP curve on the fcc side occur (such as for Fe–Ni as shown here) when alloying leads to AF or some form of low-spin exchange that coexists with the FM matrix. The lower portion of the figure shows data for the antiferromagnets fcc-Mn, fcc-Fe, fcc $Fe_{50}Mn_{50}$ and $L1_0$ NiMn (filled squares [55]). The data for pure metallic Cr is also shown. The line extrapolated from the Fe–Ni data that deviate from the SP curve to fcc-Mn nearly accommodates the data for fcc-Fe and $Fe_{50}Mn_{50}$.

Calculated values for the magnetic moment of stoichiometric Heuslers and half-Heuslers [56–58] are shown with the large filled circles that lie practically on the same curve as the 'bcc branch' of the SP curve. Experimental data for Ni–Mn–Z are shown with the smaller filled symbols [59, 55, 60–68]. These data nearly follow the SP curve with the same slope, and above a certain Z concentration, deviate from the SP curve. It is understood that the deviation occurs as AF exchange is introduced essentially through excess Mn. Deviations from the SP curve for the data of the composition series $Ni_{50}Mn_{50-x}Z_x$ is expected to follow a curve that would approach the value for $Ni_{50}Mn_{50}$.

3.2.4. Magnetic anisotropy. The occurrence of the magnetic shape-memory effect characterized with twin boundary motion relies on strong magnetoelastic coupling together with the presence of long-range FM ordering in the martensitic phase. A measure of the magnetoelastic coupling is given by the

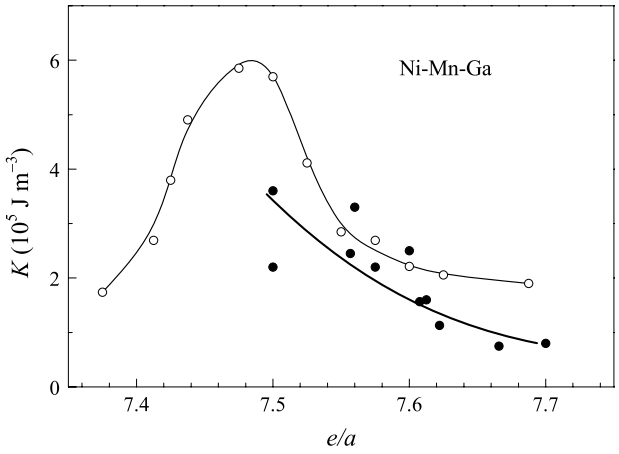

Figure 9. Magnetic anisotropy K as a function of electron concentration for Ni–Mn–Ga. Open circles: calculated, filled circles: experimental. The lines are guides.

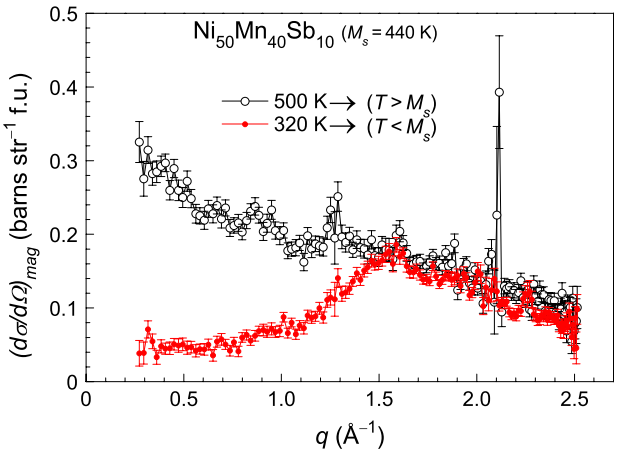

Figure 10. The magnetic cross section obtained from polarized neutron scattering at 500 and 320 K for $Ni_{50}Mn_{40}Sb_{10}$. The peak at 500 K data is related to ferromagnetic correlations and occurs at the position of the (200) nuclear Bragg peak.

magnetic anisotropy energy density K. As will be discussed in the next sections, if K is large, applying a magnetic field below saturation can set twin variants into motion by rotating them so that their magnetization easy axes tend to lie along the applied field.

Among the Ni–Mn–Z systems, substantial twin boundary motion has been observed only in Ni–Mn–Ga. For Z as a species other than Ga, very little work related to magnetic anisotropy is found in the literature. In the cubic phase, magnetic anisotropy is weak. The results of theoretical and experimental studies for martensitic Ni–Mn–Ga are collected in figure 9 from various sources [69–73, 75]. $e/a = 7.5$ corresponds to the stoichiometric Ni_2MnGa compound, and experimental data for lower values are not available. Theoretical values, calculated for $T = 0$ K, lie somewhat higher than those determined experimentally at finite temperatures for $e/a > 7.5$. Both fall with increasing e/a. Considering the fact that K increases with decreasing temperature in Ni–Mn–Ga [73], a reasonable agreement between the two methods is reached. The experimental data provided here are for the case in the orthorhombic structure with $c/a < 1$ having a short axis as the easy axis of magnetization. At higher Ni concentrations, the structure can be tetragonal with $c/a > 1$ with the easy axis lying in a plane [73]. It is worth mentioning that in alloys with excess Mn, the anisotropy decreases with increasing Mn content, due to the presence of Mn atoms with antiferromagnetic exchange [74, 75].

3.3. The nature of magnetic coupling in martensitic Heusler alloys and the role of antiferromagnetism on the martensitic transformation

Observations such as exchange bias effects [76, 77], large magnetoresistance [78, 79] and the drop in the temperature dependence of the magnetization below M_s (see figure 5) are features that suggest the presence of AF interactions in Ni–Mn-based Heusler alloys. In fact, in many cases, the presence of some form of AF coupling, especially below M_s, is frequently speculated although no direct evidence is referred to. Only neutron diffraction experiments on Ni–Mn–Sn have suggested the presence of incipient AF coupling between the Mn atoms which strengthens below M_s [80]. On the other hand, Mössbauer experiments on Ni–Mn–Sn with a small amount of ^{57}Fe give spectra just below M_s and above T_C^A that are similar [81]. This observation led to the conclusion that the occurrence of a paramagnetic state is responsible for the drop in the temperature dependence of the magnetization below M_s instead of antiferromagnetism.

More recent experiments have shown, however, that AF coupling is indeed unequivocally present both above T_C^A and below M_s down to T_C^M [82]. The antiferromagnetism is observable in the form of magnetic short-range correlations in the diffuse scattering. This is shown in figure 10 where the wavevector dependence of the magnetic scattering cross section is plotted for a $Ni_{50}Mn_{40}Sb_{10}$ alloy at 320 and 500 K. This alloy does not order ferromagnetically in the austenitic state and undergoes a martensitic transformation below 440 K. In spite of the absence of FM ordering in the austenitic state at 500 K, the presence of forward scattering indicates that FM short-range correlations are present. From the data at 320 K, one observes that, below the martensitic transformation, FM short-range correlations vanish, but the presence of strong diffuse scattering at higher q values indicate the presence of AF correlations with a broad distribution, which falls off with increasing q. Therefore, it is the occurrence of AF exchange below M_s that is responsible for the drop in the temperature dependence of the magnetization as well as for many of the observed properties mentioned above.

4. Shape-memory properties

The materials discussed in the present review have been the subject of intensive research mostly owing to the peculiar magnetomechanical properties: magnetic shape-memory and magnetic superelasticity. In the present section, we first

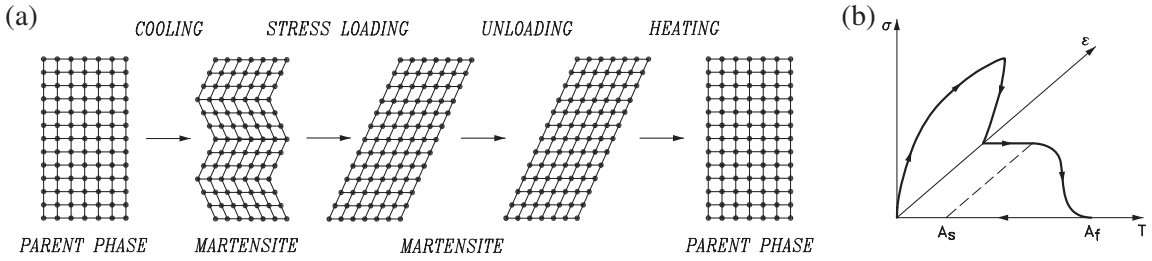

Figure 11. (a) Schematic representation of the shape-memory effect. (b) Corresponding path on the (T, σ, ϵ) space.

introduce the general features associated with shape-memory and compare them to those of magnetic shape-memory.

4.1. Shape-memory properties: general features

There are materials which are able to recover from a large deformation when heated above a certain temperature. The deformation can be of any kind (tension, bending, compression, etc) and strains as large as 10% can be recovered. Since the sample is able to recover the original shape before it was deformed, the property exhibited by this kind of a material has come to be known as shape-memory, and they are classified under the generic name of shape-memory materials [83]. Since shape-memory materials can function as sensors and actuators, they have received considerable attention as smart materials.

The property underlying the features of shape-memory alloys is the structural phase transition: the martensitic transition, a diffusionless first-order phase transition in the solid state. The lattice distortion associated with the structural change is basically described by a shear mechanism. Upon cooling, the transition occurs from a high symmetry cubic phase, known as parent phase or austenite, to a lower symmetry phase known as product phase or martensite (e.g. see figure 3). As a result of its lower symmetry, the martensitic phase is degenerate, and there are a certain number of structures which are energetically equivalent but with different crystallographic orientation: these are the martensitic domains or variants. In the absence of any generalized external field breaking the degeneracy, all variants are possible, and in the martensitic state the alloy is formed as a heterostructure resulting from the combination of several martensitic domains which are twin-related. These domains self-accommodate in such a way that the elastic energy is minimized. As pointed out in section 2.1, a major consequence of the elastic energy stored in the lattice is that the transition does not occur at a fixed (constant) temperature but rather it spreads over a certain temperature range. Also, associated with its first-order nature, a certain thermal hysteresis is present. Hence, the temperatures at the beginning and at the end of the transformation on cooling (M_s and M_f) and those corresponding to heating (A_s and A_f) are quantities commonly used to characterize the transition ('s' and 'f' refer to start and finish). Since the discovery of shape memory in Au–Cd in 1951 [84], a broad variety of materials have been found, prominent among them being the Ni–Ti alloy reported in 1963 [85]. A good compilation of the science and technology of shape-memory alloys can be found in [86].

The shape-memory effect is intimately related to the heterophase structure of the martensitic phase. The mechanism responsible for the shape memory is schematized in figure 11(a). On cooling below M_s, the martensitic phase has a polyvariant structure (for simplicity, only two variants are plotted in the figure) and, in general, almost no noticeable shape change is observed between the high-temperature and low-temperature phases owing to the small difference in the volume of the unit cell and to the self-accommodation of martensitic variants. Application of a uniaxial stress breaks the degeneracy, and by twin boundary motion those martensitic variants with favourable orientation with respect to the stress grow at the expense of other variants. This results in a macroscopic change of shape. Notice that the maximum strain is imposed by the crystallographic dimensions of the two phases. On heating the alloy above the reverse transition temperature A_f, the alloy transforms back to the cubic phase with the corresponding reversion of the martensitic domains in such a way that the original shape is recovered. In figure 11(b), we show in a stress–strain–temperature diagram the different paths associated with the above-described shape-memory mechanism.

Besides being thermally induced, the martensitic transition can also be induced by applying an external stress at a temperature above A_f. In this case, since the external stress imposes a preferred direction, the martensitic variants are no longer equivalent and the result is a martensitic phase with a single domain (the one having the higher resolved shear stress). The possibility of inducing the martensitic transition by application of a stress leads to another interesting property in shape-memory alloys: the superelasticity, which is also schematized in figures 12(a) and (b). Here, the transformation from the cubic to a single-domain martensitic phase results in a large sample deformation. Since in the absence of mechanical stress the martensitic phase is unstable at temperatures above A_f, upon unloading, the sample transforms back to the cubic phase with the associated reversion of the deformation.

In summary, it is understood that under the generic name of shape-memory properties, both the shape-memory effect and superelasticity occur in shape-memory alloys, and as to which one will occur depends on the temperature and stress ranges under study.

4.2. Magnetic shape-memory: general features

A major breakthrough in the research of shape-memory materials came about with the discovery of magnetic shape-

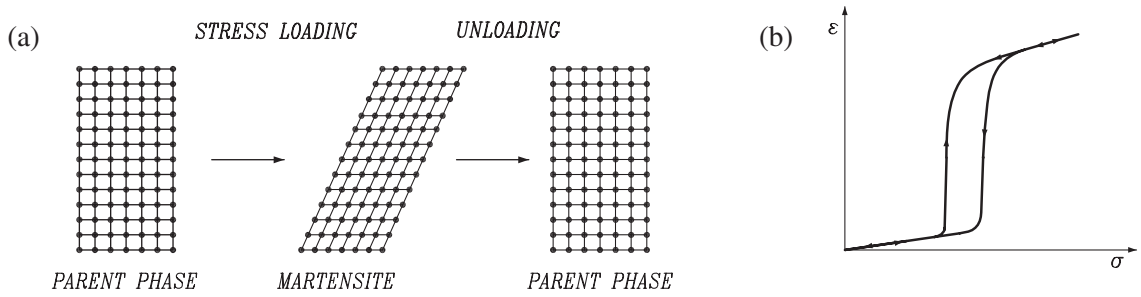

Figure 12. (a) Schematic representation of the superelastic effect. (b) Corresponding path on the (σ, ϵ) space.

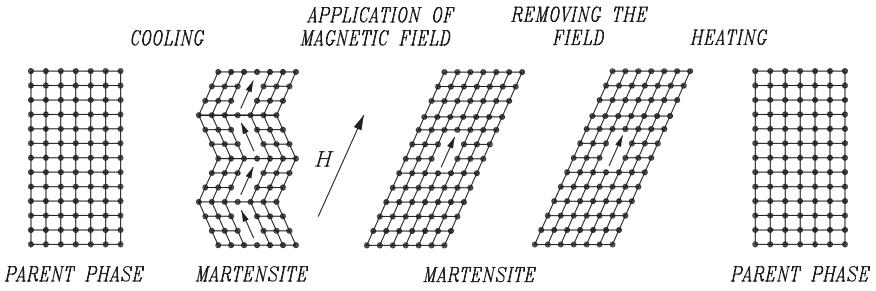

Figure 13. Schematic representation of the magnetic shape-memory effect. The arrows inside the variants indicate the corresponding direction of the easy axis. For high-enough magnetocrystalline anisotropy of the martensitic phase, applying a magnetic field causes rotation of martensitic variants.

memory alloys. Although the existence of alloys undergoing martensitic transitions within magnetically ordered phases were already known, it was the report of the possibility of inducing large recoverable strains by the application of a magnetic field which prompted the research in this field. A major inconvenience for the practical application of the shape-memory effect was the slow response of the devices inherent to the thermal control of the effect. The possibility of controlling shape memory by means of an applied magnetic field opens up a research area aimed at designing a new generation of sensors and actuators which can operate at relatively high frequencies. Additionally, since it is easier to control the magnetic field rather than the temperature, potential devices based on this effect are expected to be technologically much simpler.

The effect of a magnetic field on the dimensions of a magnetic material is a consequence of the interplay between structure and magnetic degrees of freedom. Such an interplay, which is present in all magnetic materials gives rise to small changes in the dimensions of the unit cell and is known as magnetostriction. The effects associated with magnetic shape memory originate from a different mechanism. In this case, it is a magnetostructural coupling at a mesoscopic length scale (that of magnetic and martensitic variants) which causes the length change by the re-orientation of the martensitic variants under the externally applied field. The strains achieved by this mechanism (up to 10%) are orders of magnitude larger than those corresponding to conventional magnetostriction.

Magnetic shape-memory alloys are shape-memory alloys in the conventional way as described in the previous subsection. Their specific feature is that there is an extra degree of freedom (the magnetic field) in addition to temperature and stress which can be tuned to achieve the desired functional effects. In what follows, we describe how the magnetic field affects the response of these alloys so that a parallel can be drawn between the conventional shape-memory properties and those which can be achieved by the application of a magnetic field.

4.3. Magnetic shape memory and magnetic superelasticity

The mechanism giving rise to the magnetic shape memory is sketched in figure 13. As explained in section 4.2, in the martensitic state, the sample is a heterophase composed by several twin-related martensitic variants (structural domains). For simplicity, only two of these domains are shown in figure 13. Below the Curie point there are magnetic domains within each martensitic variant with the magnetization pointing along the easy axis and organized in such a way that they minimize the magnetostatic energy [87–89]. When a magnetic field is applied, there is the tendency of the magnetic moments to align along the magnetic field. If the magnetic anisotropy is weak, the magnetic moments will rotate within each martensitic variant. This will result in almost no change in the sample dimensions other than those corresponding to conventional magnetostriction. However, if the magnetic anisotropy is high, rotation of magnetic domains requires a significant increase in magnetic energy. Provided that the energy to move twin boundaries is low enough, there will be a rotation of the structural domains in such a way that their easy axis becomes aligned with the externally applied field. In this case, the rotation of martensitic variants is promoted by the difference in the Zeeman energy between the variants, and the result is a significant change in the dimensions of the sample [90]. In this process, the magnetic field plays

the role that mechanical stress plays in conventional shape-memory alloys in the sense that application of an external field results in a large deformation of the sample. Shape memory is achieved on heating the alloy above the reverse martensitic transition temperature, where all martensitic variants disappear and the sample recovers its original shape. Since in magnetic alloys deformation is achieved by applying a magnetic field, this effect has been termed magnetic shape memory.

In general, the strain achieved by the rotation of martensitic variants under an applied field is not recovered when the magnetic field is removed. Only for very small strains, reversibility of shape change with field has been reported [9]. In addition to heating the sample, there are other ways of recovering the strain induced by applying a field. One possibility is to rotate the magnetic field. Another possibility, which is the most commonly used in magnetic shape-memory actuators, is to apply a mechanical stress perpendicular to the direction of the field. In the absence of magnetic field, martensite is in a single-variant state, corresponding to that variant which is favoured by the stress. On applying a magnetic field along the hard axis, the Zeeman energy tends to orient the magnetization along the field, and for large-enough fields the martensitic variants rotate so as to align their easy axis along the external field. In this way, the sample transforms from a single-variant martensite to a different single-variant martensite resulting in a large strain. When the magnetic field is removed, the sample reverts to the martensitic state imposed by the applied load so that the original shape is recovered. Under a proper choice of the directions of the load and magnetic field, thereby selecting the particular sets of martensite variants, strains as large as 10% can be obtained [91].

As previously mentioned, the magnetic shape memory relies on a balance between the magnetic energy and the energy required for twin boundary motion [92]. In a general way, such a balance is expressed as [93]

$$\Delta E \geqslant \epsilon_0 \sigma_{\mathrm{tw}}, \tag{25}$$

where ΔE is the magnetic energy difference between differently oriented adjacent twin variants, ϵ_0 is the tetragonal distortion and σ_{tw} is the twinning stress. If the material is magnetized to saturation with the magnetization perpendicular to the easy axis of one variant and along the axis of the adjacent variant, the difference of the magnetic energy is equal to the difference of the magnetic anisotropy. Then, the general condition for twin boundary motion is expressed as

$$\sigma_{\mathrm{mag}} = K/\epsilon_0 \geqslant \sigma_{\mathrm{tw}} + \sigma_{\mathrm{ext}}, \tag{26}$$

where K is the magnetic anisotropy constant and σ_{ext} is the external applied stress. This equation reflects the fact that high magnetic anisotropy and/or high twin boundary mobility are requisites for the occurrence of magnetic shape memory that will take place when the magnetic stress σ_{mag} is larger than the mechanical stress [94]. It also shows that too large external stresses will also inhibit twin boundary motion.

So far, we have discussed the mechanisms of magnetic shape memory which rely on a coupling between magnetism and structure at a mesoscopic level. By pursuing the parallelism with conventional shape-memory alloys, we discuss here the general features of the magnetic equivalent to superelasticity, i.e. magnetic superelasticity. This effect is schematized in figure 14 and it corresponds to the achievement of large strains by the occurrence of the martensitic transition induced by the application of a magnetic field. Upon removal of the field, the reverse transition takes place with the consequent recovery of the strain. Notice that this mechanism does not rely on twin boundary motion but is based on the possibility of inducing the martensitic transition on applying a magnetic field. Such a possibility is promoted by the magnetic field dependence of the transition temperature. This mostly relies on a coupling between structure and magnetism at a microscopic level modifying the relative phase stability between the martensitic and the austenitic phases. The application of magnetic field will stabilize the phase having a higher magnetization. Therefore, forward or reverse martensitic transitions can be induced by applying a magnetic field depending on whether martensite has a higher or lower saturation magnetization than austenite, as was shown in figure 5. Figure 14(a) illustrates the forward magnetic superelasticity, while figure 14(b) illustrates the reverse magnetic superelasticity. Upon removing the field, the opposite transition will occur with a certain hysteresis. Forward magnetic superelasticity will result in a significant reversible change in the sample dimensions, because a single martensite variant is formed. Conversely, for the reverse magnetic superelasticity, no significant shape change is expected. However, in the latter case, a change in the sample dimensions will occur provided that a noticeable difference in the volume of the unit cells of the austenite and martensite exists.

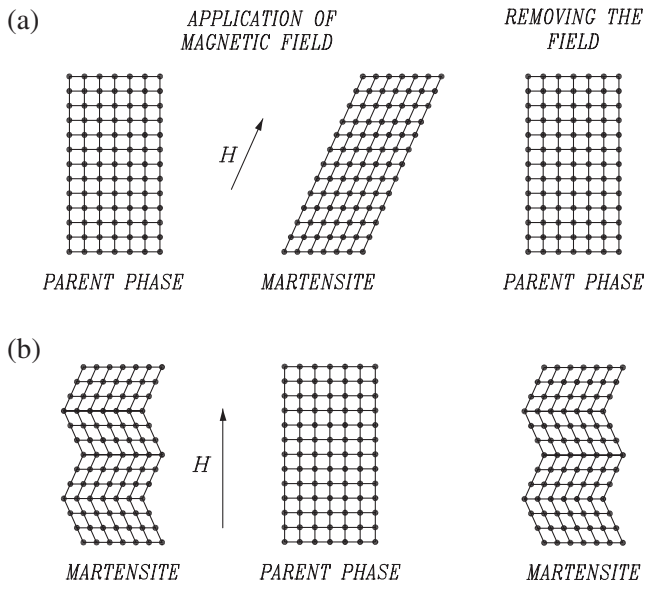

Figure 14. Schematic representation of the magnetic superelastic effect. (a) The application of a field shifts the transition to a higher temperature, thus inducing the forward martensitic transition. (b) The application of a field shifts the transition to a lower temperature, thus inducing the reverse martensitic transition.

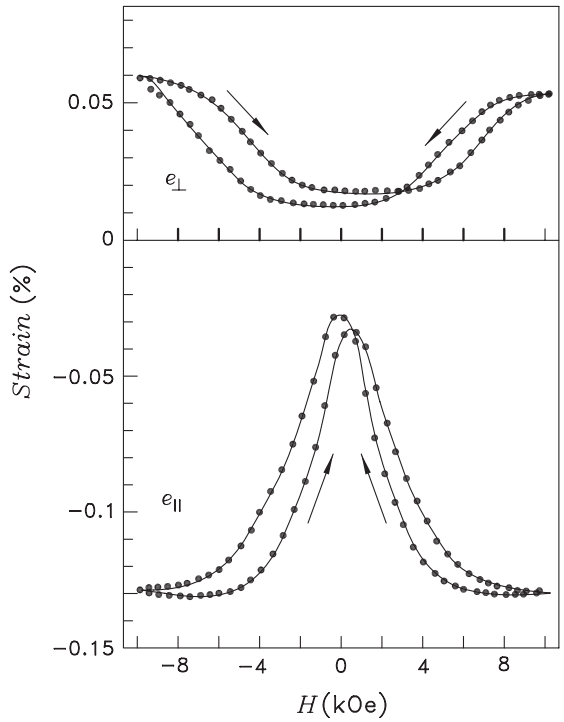

Figure 15. Strains measured along the [001] direction, induced in the martensitic phase for fields applied along the [001] ($e_\parallel$) and along the [110] ($e_\perp$) directions as a function of the magnetic field in a Ni_2MnGa single crystal. The indicated directions refer to the cubic phase. Figure adapted from [9].

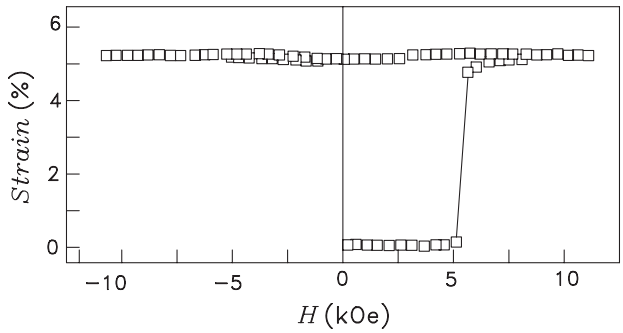

Figure 16. Strain versus applied field in an $Ni_{48.8}Mn_{28.6}Ga_{22.6}$ single crystal. Figure adapted from [95]. The sample was pre-stressed to obtain a single martensite variant state with the *c* axis along the direction of the stress. Magnetic field was applied perpendicular to the *c* axis (easy axis) of the martensitic phase. The strain was measured along the direction of the stress (perpendicular to the field).

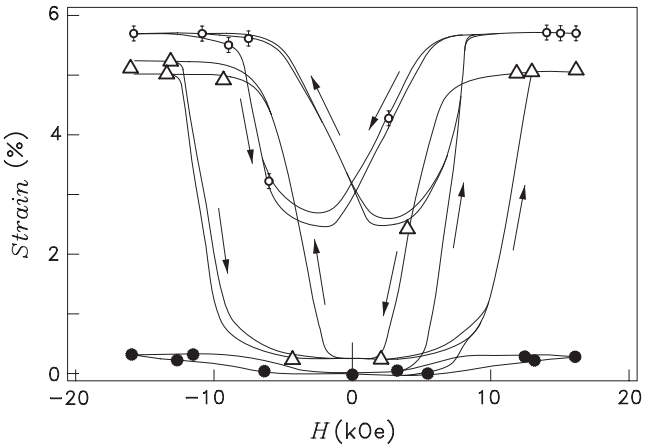

Figure 17. Strain versus applied field in an $Ni_{51.1}Mn_{24.0}Ga_{24.9}$ single crystal. A compressive stress was applied along the [100] direction of the cubic phase and magnetic field was applied along the [011] direction of the cubic phase. Strain was measured in the direction of the applied stress (perpendicular to the field). Open circles 2 MPa, triangles 4 MPa and solid circles, 6 MPa. Figure adapted from [96].

Magnetic superelasticity is expected to occur in those alloys exhibiting large shifts in the martensitic transition temperature with magnetic field. This condition can be expressed in terms of the Clausius–Clapeyron equation (e.g. (12)), which shows that such shifts will be particularly relevant for those alloys with a saturation magnetization in the austenite that is markedly different from that of the martensite.

4.4. Magnetic shape memory and magnetic superelasticity: selected illustrative results

Figures 15–18 illustrate several situations related to magnetic shape memory. The pioneering data for the stoichiometric Ni_2MnGa are reproduced in figure 15 [9]. The sample is a single crystal and no external stress is applied. A small recoverable magnetic-field-induced strain is observed along parallel and perpendicular directions of the magnetic field. Large strains are achieved by pre-stressing (3 MPa) the sample in the martensitic state to obtain a single-variant martensitic state. As illustrated in figure 16 [95], the application of a magnetic field generates a large strain caused by twin boundary motion towards an almost single-variant martensitic state having a magnetic easy axis parallel to the field. The large strain is not recovered on removing the field. In order to recover the strain, it is necessary to maintain the stress applied to the sample while the magnetic field is swept. This is shown in figure 17 [96] for several uniaxial stresses applied perpendicular to the magnetic field. Results also show that as the external stress exceeds a certain value, the amount of recoverable strain diminishes, since the magnetic energy is not large-enough to overcome the elastic energy. When the stress is applied parallel to the magnetic field, the recoverable strain is much lower than in the perpendicular configuration as illustrated in figure 18 [97].

The occurrence of variant re-orientation by twin boundary motion under the application of a magnetic field has been demonstrated by means of several experimental techniques. The combination of optical and scanning microscopy with several magnetic imaging techniques has enabled a simultaneous observation of magnetic and structural domains (variants) [98, 99, 93]. While twin boundary motion has unambiguously been proven to occur, there is some controversy as to whether there is magnetic domain wall motion within the martensitic variants [96, 93, 100, 89]. From a more microscopic viewpoint, neutron diffraction studies have also revealed magnetic-field-induced martensite re-orientation [101, 102].

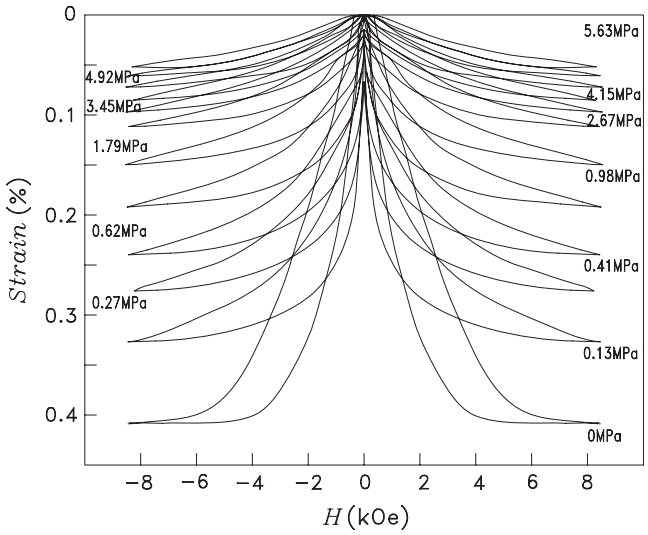

Figure 18. Strain versus applied field in an $Ni_{50}Mn_{28.7}Ga_{21.3}$ single crystal. A uniaxial load was applied collinearly to the magnetic field along the [001] direction of the cubic phase. Strain was also measured along the [001] direction. Figure adapted from [97].

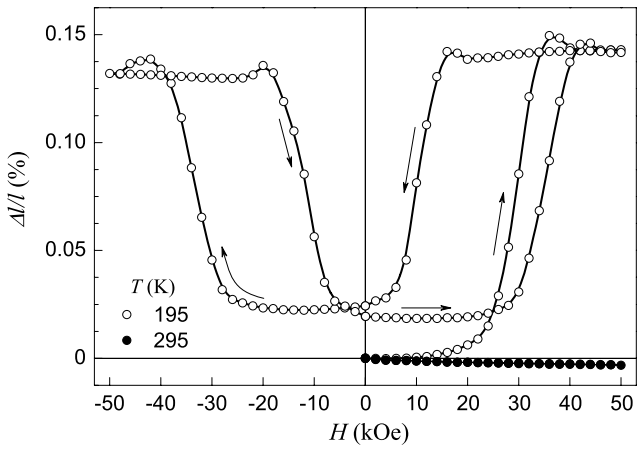

Figure 19. Relative length change as a function of magnetic field in polycrystalline $Ni_{50.3}Mn_{33.7}In_{16.0}$ in the martensitic (open symbols) and austenitic states (solid symbols). Strain was measured in a direction parallel to the magnetic field. Data from [108].

Magnetic superelasticity has been reported for a number of magnetic shape-memory alloys. An example is shown in figure 19 for an Ni–Mn–In polycrystal. Magnetic field is applied isothermally at a temperature close to $A_s = 195$ K for the sample given in the figure. As the field exceeds a certain value, there is a considerable length change of the sample associated with the transformation from a multi-variant martensite to austenite. Upon removal of the field, the sample recovers its original length with a certain field hysteresis as a consequence of the transformation from austenite to multi-variant martensite. This process is completely reproducible on cycling and the marginal difference in $\Delta l/l$ from the first cycle is likely to be due to a slightly different variant configuration of the virgin state. Application of magnetic field at a temperature above A_f results in a very small length change (solid symbols) originating from the magnetostriction of the

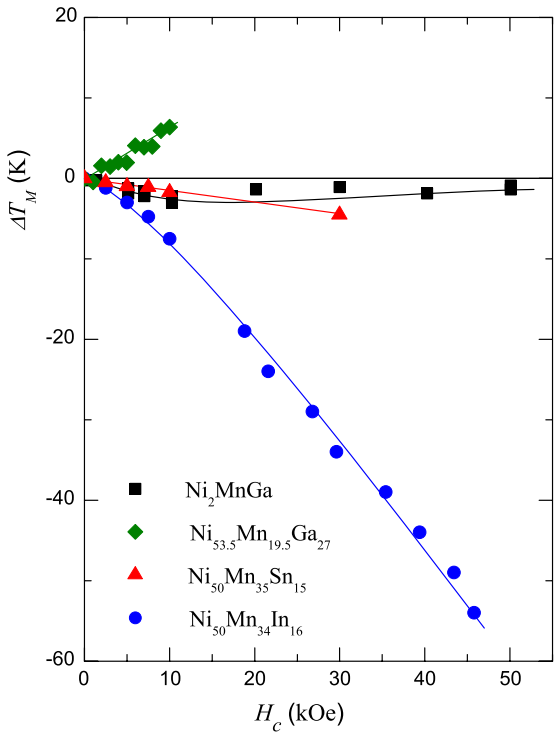

Figure 20. Shift in the martensitic transition temperature as a function of magnetic field for several Ni–Mn–Z alloys. For Ni_2MnGa we have used data from [105], for $Ni_{53.5}Mn_{19.5}Ga_{27}$ from [106], for $Ni_{50}Mn_{35}Sn_{15}$ from [107] and from [108] for $Ni_{50}Mn_{34}In_{16}$.

austenitic phase. Notice the parallelism between magnetic superelasticity (figure 19) and conventional superelasticity depicted in figure 12.

The possibility of achieving field-induced strains by means of magnetically inducing the reverse martensitic transition has also been termed as metamagnetic shape memory [103]. An Ni–Mn–In–Co single crystal was pre-stressed to select a single martensitic variant and the application of a magnetic field caused a giant strain associated with the transition from single-variant martensite to an austenitic single crystal [104]. Such a giant strain is not expected to be reversible, since on removing the field, a multi-variant martensite state will be formed in the absence of any external stress breaking the degeneracy of the martensitic phases.

As previously mentioned, magnetic superelasticity relies on the possibility of the transition to be induced by the magnetic field and requires a significant shift in the transition temperature with field. In figure 20 we have compiled the shift in the transition temperature with field for several Ni–Mn–Z alloys [105–108]. For Ni–Mn–Ga, the data correspond to the alloy which has been reported to exhibit the largest shift [106]. In this case, there is a relatively large increase in the transition temperature with field, in agreement with the larger saturation magnetization of the martensite. For Ni–Mn–In and Ni–Mn–Sn the transition temperature decreases with increasing field, in agreement with the lower value of the magnetization in the martensitic state. The largest shift observed for $Ni_{50.3}Mn_{33.8}In_{15.9}$ is associated with a significant

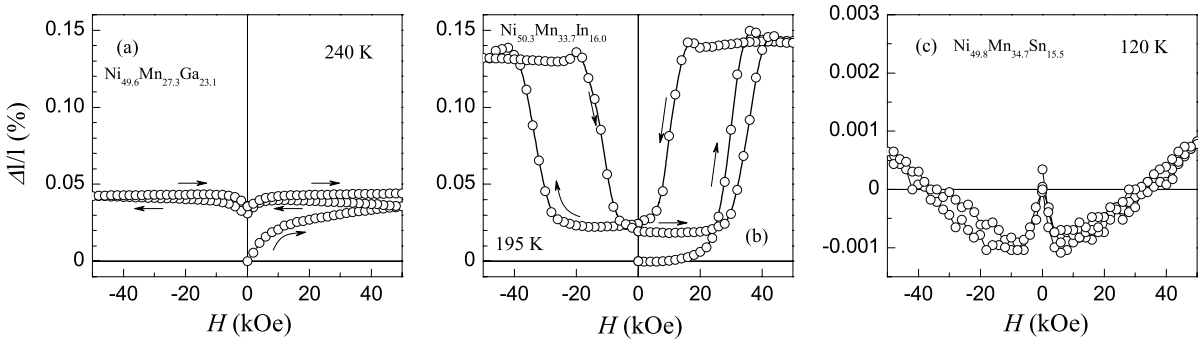

Figure 21. Relative length change as a function of magnetic field illustrating the shape-memory effect (a), magnetic superelasticity (b) and conventional magnetostriction (c) in several polycrystalline Ni–Mn–Z samples. Strain was measured in a direction parallel to the magnetic field.

magnetization change at the transition (see figure 5) and also with a low entropy change.

The occurrence of the magnetic-field-induced martensitic transition has been confirmed by x-ray and neutron diffraction experiments under magnetic field for several alloy systems. While only a small change in the relative amount of martensitic and cubic phases was obtained from Rietveld analysis of the neutron diffraction patterns of $Ni_{2.19}Mn_{0.81}Ga$ [109], clear evidence of the reverse martensitic transition has been reported from x-ray powder diffraction in $Ni_{50}Mn_{36}Sn_{14}$ [110], neutron powder diffraction in $Ni_{49.7}Mn_{34.3}In_{16.0}$ [108] and high-energy synchrotron x-ray diffraction in $Ni_{45}Co_5Mn_{36.6}In_{13.4}$ [111].

The response in strain of a given alloy to the magnetic field will strongly depend on the dominant mechanism of the magnetoelastic coupling, as illustrated in figure 21 for several polycrystalline alloy systems. In the case of $Ni_{49.6}Mn_{27.3}Ga_{23.1}$, the strong magnetocrystalline anisotropy makes the rotation of magnetic domains possible, giving rise to a length change. Since the martensitic transition depends weakly on magnetic field, there is no strain arising from a magnetic-field-induced transition for this alloy. As discussed in section 3.2.4, magnetic anisotropy decreases with increasing Mn content, and for this reason no magnetic shape-memory effect occurs in Ni–Mn–Ga with high Mn content. By contrast, in $Ni_{50.3}Mn_{33.7}In_{16.0}$, the magnetic field induces the reverse martensitic transition giving rise to significant strain. The strain is recoverable upon removal of the field. In this case, there is considerable hysteresis associated with the first-order character of the magnetic-field-induced transition. On the other hand, there is no twin boundary motion for this alloy, probably due to a low magnetic anisotropy in the martensitic phase. Finally, for $Ni_{49.8}Mn_{34.7}Sn_{15.5}$, applying a magnetic field up to 50 kOe does not result in twin boundary motion or a field-induced martensitic transition. In this case, the magnetic field dependence of the transition temperature is not large enough for the reverse transition to be induced and magnetic anisotropy of the martensitic phase is weak. The recorded strain, which is two orders of magnitude lower than that in the previous cases, corresponds to conventional magnetostriction in the martensitic phase.

The strain arising from magnetic superelasticity shown in figures 19 and 21(b) corresponds to the length change from

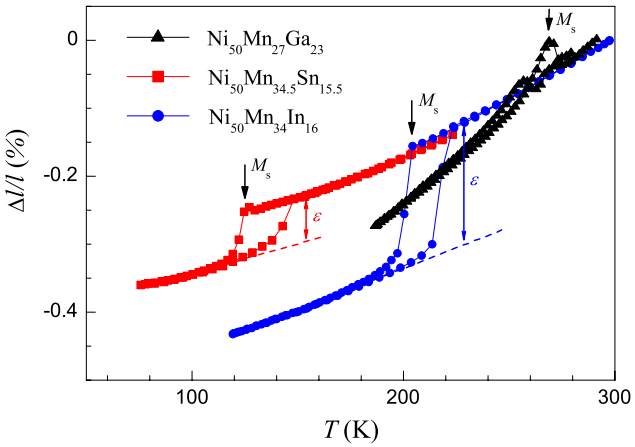

Figure 22. Relative length change as a function of temperature for $Ni_{50}Mn_{27}Ga_{23}$, $Ni_{50}Mn_{34.5}Sn_{15.5}$ and $Ni_{50}Mn_{34}In_{16}$ polycrystalline samples at zero applied magnetic field.

a multi-variant martensite to a cubic state. In principle, due to the self-accommodating nature of the martensitic state, the expected strain would be very small unless there is a volume change between austenite and martensite. This is precisely the case for Ni–Mn–Sn and Ni–Mn–In as illustrated in figure 22. A significant relative length change at the transition is measured in contrast to Ni–Mn–Ga, for which only a small length change occurs at the transition. Accurate determination of the martensitic and cubic structures in Ni–Mn–Sn from neutron diffraction experiments [80] have confirmed a ∼0.5% relative volume change, while the volume change for Ni–Mn–Ga is negligible. The value obtained from neutron data is in good agreement with the estimation ($\Delta v/v_0 \sim 3\epsilon$) from the data in figure 22.

One of the inconveniences for practical applications of the magnetic shape-memory effect is the low value of the output stress achieved by the mechanism of variant re-orientation. As expressed by equation (26) and shown in figures 17 and 18, even at large magnetic fields, the driving force is limited by the magnetic anisotropy energy. Magnetic-field-induced strain is inhibited when stresses above a few MPa are applied to the sample. Very recently, it has been argued that for small-enough specimens, such a blocking stress can be considerably

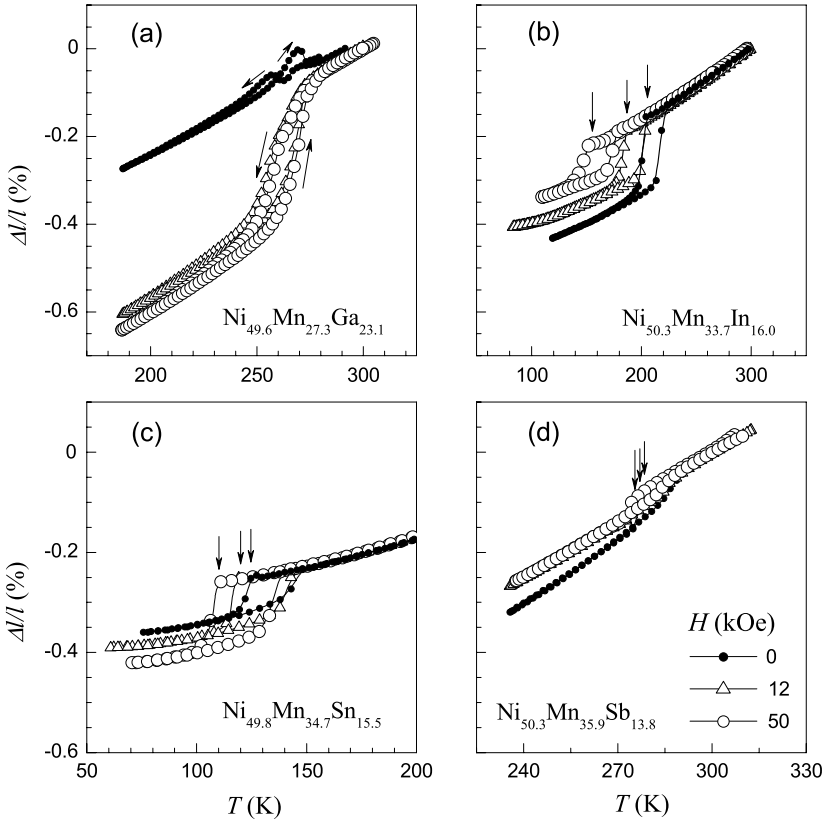

Figure 23. Relative length change as a function of temperature and selected values of the applied magnetic field in (a) $Ni_{49.6}Mn_{27.3}Ga_{23.1}$, (b) $Ni_{50.3}Mn_{33.7}In_{16.0}$, (c) $Ni_{49.8}Mn_{34.7}Sn_{15.5}$ and (d) $Ni_{50.3}Mn_{35.9}Sb_{13.8}$ polycrystalline samples. Strain was measured in a direction parallel to the magnetic field. Vertical arrows in (b)–(d) indicate the martensitic start temperature.

increased [112]. A convenient way to circumvent this problem is to take advantage of the magnetic superelastic effect. It has been shown that in a Co-doped Ni–Mn–In single crystal [104] the output stress generated by the magnetic-field-induced reverse martensitic transition can be as high as 100 MPa.

4.5. Effect of magnetic field on thermally induced martensite

In the previous sections, we have discussed the effect of an isothermal application of a magnetic field. Here we consider how the thermally induced martensitic transition is affected by the application of a magnetic field, i.e. we focus on the effect of a magnetic field in the nucleation (and growth) of martensite. It is expected that owing to magnetoelastic coupling, the application of a field breaks the degeneracy of the low-temperature martensitic phase in such a way that those martensitic variants with an easy axis oriented along the field will nucleate easier than the other variants. This effect will cause differences in the strain versus temperature curves recorded under zero field and under an applied field. Indeed, this has been reported for Ni–Mn–Ga single crystals [113] and polycrystals [73]. Moreover, calorimetric measurements under a magnetic field have revealed differences in the kinetics of the martensitic transition and in the dissipated energy [12]. It was found that the area within the hysteresis loop increased on increasing the magnetic field, thus reflecting an increase in the dissipated energy with field. This is associated with the tendency of the system to nucleate a single variant of martensite.

In figure 23, we compare the effect of magnetic field on the formation of martensite for different Ni–Mn–Z polycrystalline compounds [45]. The relative length change at the martensitic transition is significantly modified under the presence of an applied magnetic field. The different behaviour originates from a preferred nucleation of those martensitic variants with their easy axis pointing along the field direction. For Ni–Mn–Ga and Ni–Mn–Sn, the relative length change under an applied field is larger than without a field, while for Ni–Mn–In and Ni–Mn–Sb, the effect of the field is to reduce the relative length change between martensite and the cubic phase. It is, therefore, expected that for Ni–Mn–Ga and Ni–Mn–Sn, the easy axis is along a short axis while, for Ni–Mn–In and Ni–Mn–Sb, the easy axis should be along a long axis of the martensitic unit cell. While magnetic anisotropy measurements for Ni–Mn–Ga [114, 73] support this assumption, at present no magnetic anisotropy data are available for the other alloy systems.

For Ni–Mn–Sn and Ni–Mn–In alloys with low martensitic transition temperatures [115, 116] and also for the quaternary NiCoMnIn alloy [117], it has been reported that cooling under magnetic field causes a kinetic arrest of the martensitic transition, i.e. a considerable amount of the cubic high-temperature phase is retained at very low temperatures. Although kinetic arrest effects could in principle influence the relative length change at the martensitic transition, the results

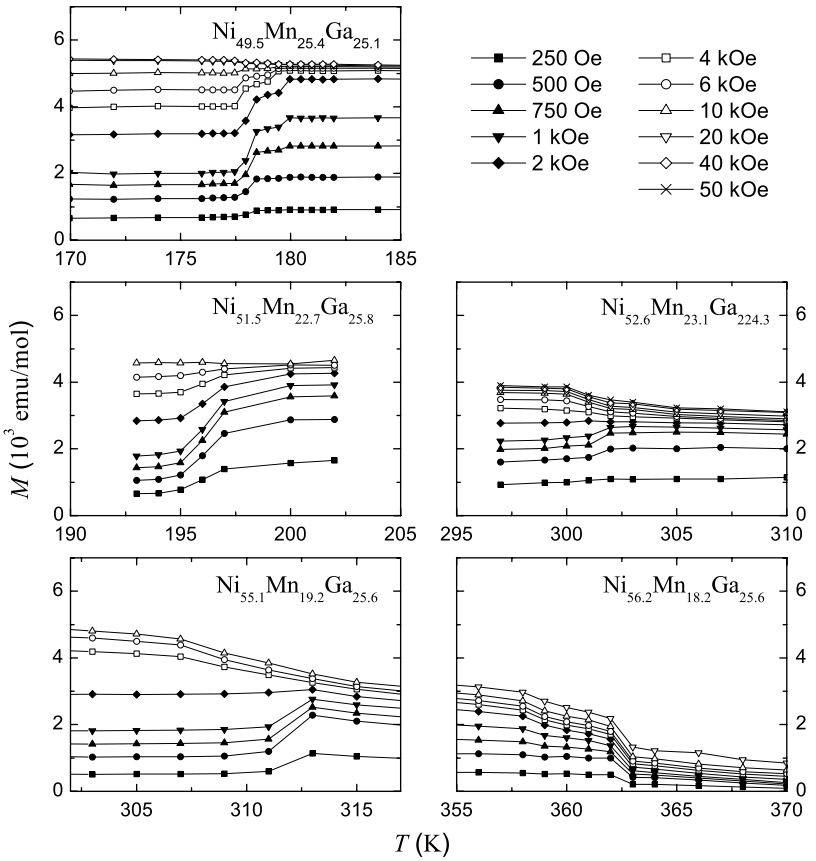

Figure 24. Magnetization versus temperature for Ni–Mn–Ga alloys of selected compositions at given values of the applied magnetic field. For the selected alloys data have been taken from the references given in table 1.

in figure 23 cannot be interpreted in terms of a retained cubic phase. On the one hand, for Ni–Mn–In, kinetic arrest is only expected for high fields (larger than 40 kOe) [115]. On the other hand, and more significantly, the relative length change should decrease with increasing field for all alloy systems. This is not the case for Ni–Mn–Sn and Ni–Mn–Sb. Therefore, the most likely cause for the modification in the relative length change at the martensitic transition is the preferred nucleation of martensitic variants.

5. Magnetocaloric properties

This section is devoted to presenting the key features of the magnetocaloric properties which are intimately related to the martensitic transition in magnetic shape-memory alloys. It is shown that these magneto-thermal properties have the same physical origin as the magnetomechanical properties discussed in section 4. Firstly, we will focus on Ni–Mn–Ga and then on other Heusler shape-memory materials.

5.1. Magnetocaloric effect in Ni–Mn–Ga

In figure 24 we present magnetization data as a function of temperature for fixed values of the magnetic field for Ni–Mn–Ga alloys of selected compositions close to the $Ni_{50+x}Mn_{25-x}Ga_{25}$ line, listed in table 1. Alloy 1 has a composition close to stoichiometric Ni_2MnGa, and the remaining have compositions with a deficiency of Mn. Data have been extracted from published isothermal magnetization curves measured following a sequence of increasing temperatures. In all cases, the magnetization displays a significant change, $\Delta M(H) = M_M - M_P$ (M_M and M_P are the magnetization in the martensitic and parent phases, respectively) at the martensitic transition. The change is not abrupt but rather it extends over the temperature range where coexistence between both parent and martensitic phases occur. The field dependence of $\Delta M(H)$ is shown in figure 25. Except for alloy 5 (with $T_M \sim T_C$), ΔM is negative for small fields and shows a minimum at H_M. For larger fields, ΔM increases with increasing field and reaches a positive saturation value ΔM_{sat}. For alloy 5, ΔM monotonically increases with increasing H up to saturation. The increase towards saturation approximately follows an exponential behaviour characterized by a field H_s. The saturation value determines the difference of magnetic moments between martensite and parent phases. From the magnetization data, the field-induced entropy change, $\Delta S(T, H)$, can be obtained (see equation (21)). An example is given in figure 26. In this example, the peak structure displayed by ΔS reflects the fact that the martensitic transition occurs through discrete jumps. The associated average field-induced entropy change, $\langle \Delta S(H) \rangle$, is obtained using equation (13). The effective temperature range of the transition, $\overline{\Delta T(H)}$, has been estimated as the width of the peak in the corresponding $\Delta S(T, H)$ curves (see figure 26). In figure 27, we show $\langle \Delta S(H) \rangle$ for the Ni–Mn–Ga

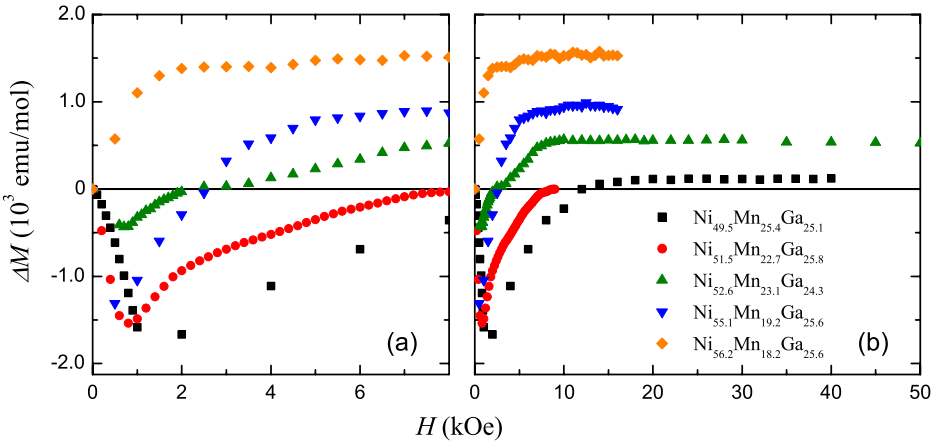

Figure 25. Magnetization change ΔM at the martensitic transition as a function of the magnetic field for the Ni–Mn–Ga samples listed in table 1. (a) Detail of the low applied magnetic field range. (b) Whole range of applied fields.

Table 1. Data corresponding to the analysed Ni–Mn–Ga alloys: bibliographic reference, atomic composition, valence electron concentration (e/a) and transition temperatures (T_M and T_C).

Alloy[a]	Ref.	at.% Ni	at.% Mn	at.% Ga	e/a	T_M (K)	T_C (K)	$T_C - T_M$ (K)
1	[12]	49.5	25.4	25.1	7.48	180	381	201
2	[10]	51.5	22.7	25.8	7.51	197	351	154
3	[11]	52.6	23.1	24.3	7.61	297	345	48
4	[14]	55.2	19.2	25.6	7.63	310	335	25
5	[14]	56.2	18.2	25.6	7.66	361	361	∼0

[a] Alloys 1 and 3 are single crystals; the others are polycrystals.

alloys listed in table 1. In all cases, the observed behaviour is very similar: the entropy change first increases with increasing H, then reaches a maximum and finally it decreases linearly at higher fields. Except for alloys 1 and 2, the initial increase of $\langle \Delta S \rangle$ is weak and is not even observed for alloy 5 (for which $T_M \sim T_C$). The initial increase in $\langle \Delta S(H) \rangle$ is related to the decrease in $\Delta M(H)$ observed in low applied fields. At high fields, $\langle \Delta S(H) \rangle$ decreases linearly with increasing field. The magnitude of the maximum (strength of the inverse magnetocaloric effect) tends to decrease with increasing e/a (see table 1). This is in agreement with reported results for a Ni–Mn–Ga alloy with very low $e/a = 7.3$ (low content of Mn) for which a maximum value of about 0.35 J mol^{-1} K^{-1} has been obtained at a field of 2 kOe [118]. In this alloy, the change from inverse to conventional magnetocaloric effect has been observed below 30 kOe. This non-monotonic behaviour of ΔM and $\langle \Delta S(H) \rangle$ can be understood by taking into account the role of the magnetic anisotropy on the martensitic microstructure formed at the transition under an applied magnetic field [13] as illustrated in figure 28. At zero or very low applied field, the martensite consists of a series of twin-related variants. In each variant, magnetic domains are formed in such a way that the magnetization alternates between two opposite values along the corresponding easy axis. As previously mentioned, this up–down configuration of magnetic moments is precisely arranged to yield no poles on twin boundaries. For large-enough fields, magnetic domains tend to coincide with twin bands. In this range of fields, owing to the strong magnetocrystalline anisotropy of the martensitic phase,

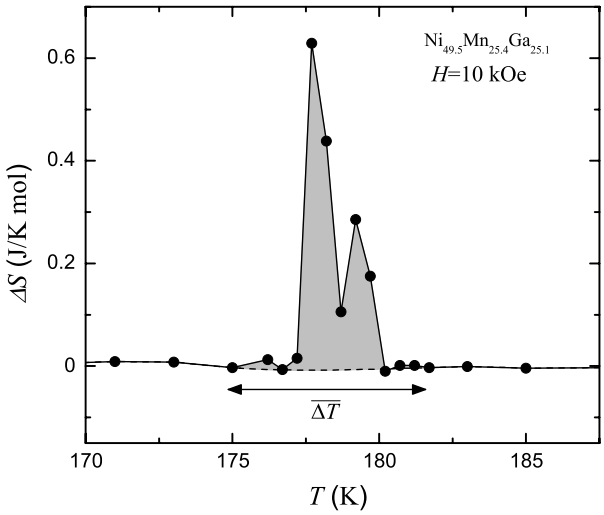

Figure 26. Field-induced entropy change as a function of temperature for an applied field of 10 kOe in $Ni_{49.5}Mn_{25.4}Ga_{25.1}$. The shaded area corresponds to $\int_{\overline{\Delta T}} \Delta S(T, H)\, dT$. $\langle \Delta S(H) \rangle$ is obtained as this area divided by $\overline{\Delta T}$. The estimation of $\overline{\Delta T}$ is shown.

the Zeeman energy difference between neighbouring variants is minimized by increasing the fraction of variants with their easy magnetization axis forming a smaller angle with the applied field. Finally, for high-enough fields, a magnetically saturated single-variant martensitic crystal should result. In practice, the single-variant saturated state is only reached for suitable initial states. The mechanism described is,

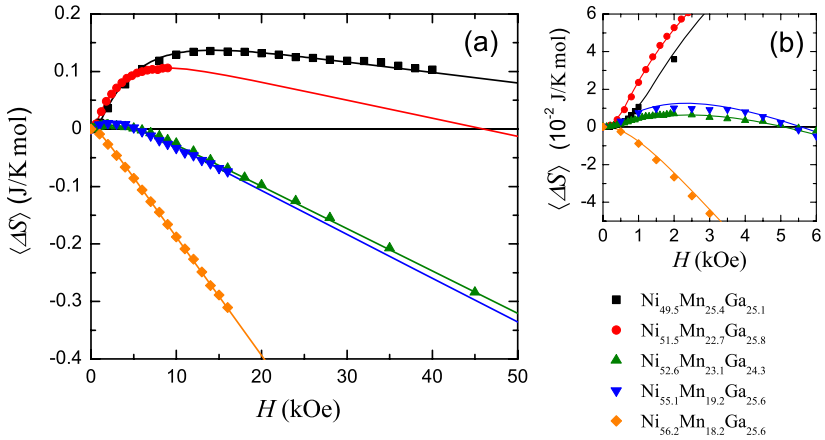

Figure 27. (a) Dependence of the average field-induced entropy change, $\langle \Delta S \rangle$, on the applied magnetic field for the Ni–Mn–Ga alloys listed in table 1. The symbols correspond to values obtained from experimental data. Continuous lines are guides to the eyes. (b) Detail of the low applied magnetic field region.

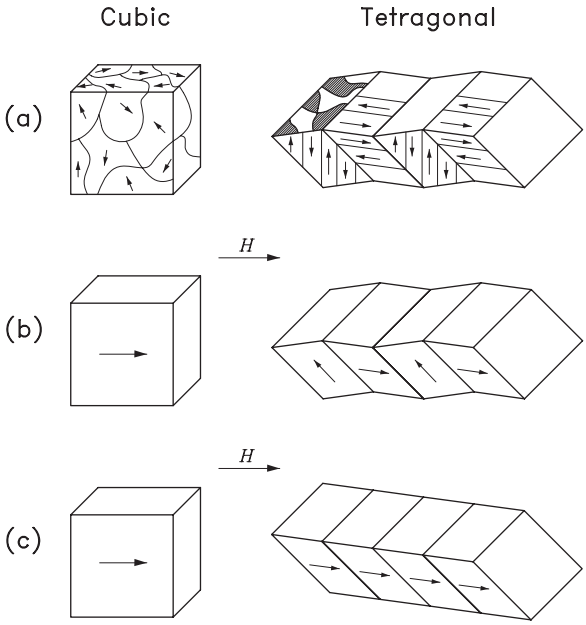

Figure 28. Schematic illustration showing the influence of a magnetic field on the magnetostructural pattern that results from the martensitic transition in a magnetic shape-memory alloy at different values of the applied magnetic field. It is assumed that the parent phase is magnetically isotropic while the martensite shows strong uniaxial magnetocrystalline anisotropy. The arrows indicate the direction of the magnetic moment within each magnetic domain. Within martensitic variants the magnetic moment points along the corresponding easy axis. (a) Very low applied field. (b) Intermediate fields. (c) Strong fields.

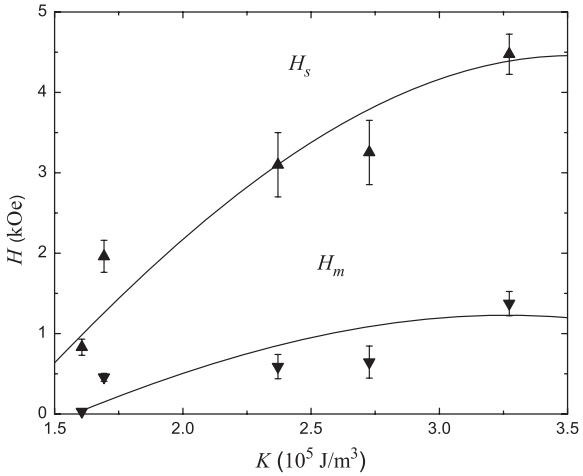

Figure 29. Dependence of the characteristic fields H_s and H_M on the anisotropy constant K for the set of alloys listed in table 1. The fields have been estimated from ΔM versus H data shown in figure 25. Continuous lines are guides to the eyes.

indeed, related to the same coupling mechanism that yields the magnetic shape-memory effect as discussed in section 4.3. It is worth noting that the amount of decrease of ΔM in the range of low fields is reduced as T_M approaches T_C, i.e. on increasing e/a (see figure 25). This behaviour is in agreement with the observed decrease of magnetic anisotropy K with increasing e/a as depicted in figure 9. Moreover, consistent with this result, the fields H_M and H_s increase with increasing K (see figure 29).

The results presented above confirm that in Ni–Mn–Ga (and in general in Heusler alloys), the magnetocaloric effect originates from two different contributions: (i) the coupling controlled by strong uniaxial magnetic anisotropy of the martensitic phase, which takes place at the length scale of martensite variants and magnetic domains (extrinsic effect), and (ii) the intrinsic microscopic coupling related to the change of magnetic moment induced by the change of symmetry which occurs at the transition. The behaviour described above for Ni–Mn–Ga has also been found for Ni–Fe–Ga alloys, which also have been reported to exhibit an inverse magnetocaloric effect at low fields due to magnetic anisotropy effects. In the latter case, entropy changes are slightly lower than in Ni–Mn–Ga alloys [119].

5.2. Results for other Heusler magnetic shape-memory alloys

In this section we focus our attention on the magnetocaloric properties exhibited by the Ni–Mn–Z family, with Z different

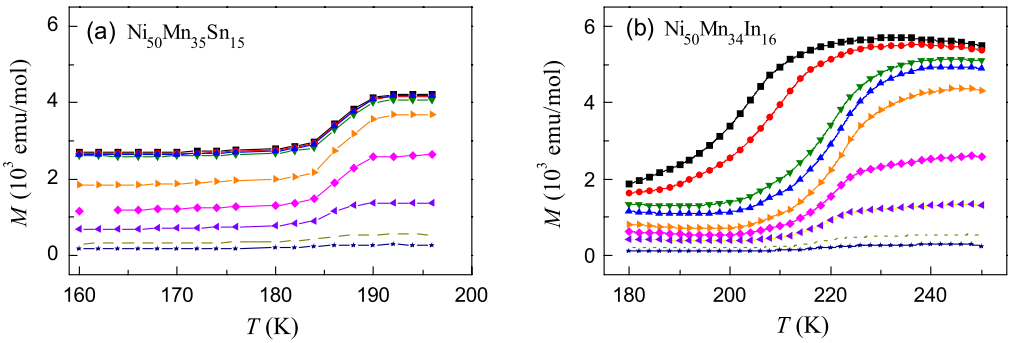

Figure 30. Magnetization versus temperature in the vicinity of the martensitic transition at selected values of the applied magnetic field. (a) $Ni_{50}Mn_{35}Sn_{15}$. From bottom to top, $H = 0.1, 0.2, 0.5, 1, 2, 10, 50$ kOe. (b) $Ni_{50}Mn_{34}In_{16}$. From bottom to top, $H = 0.1, 0.5, 2, 5, 10, 20, 30, 40, 50$ kOe.

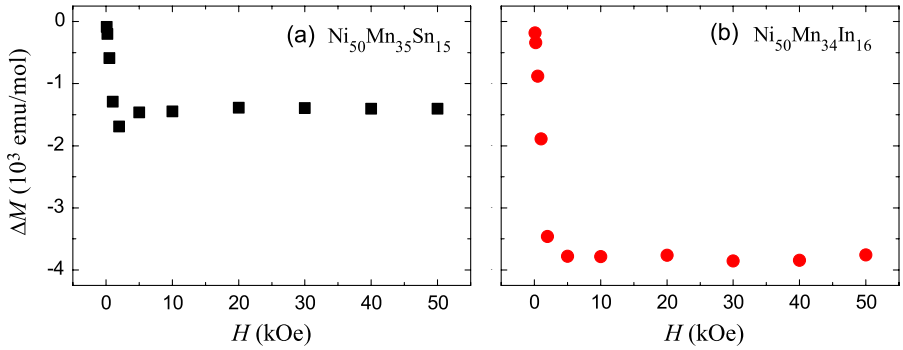

Figure 31. Magnetization change at the martensitic transition as a function of the magnetic field for (a) $Ni_{50}Mn_{35}Sn_{15}$ and (b) $Ni_{50}Mn_{34}In_{16}$.

from Ga. Special attention will be paid to alloys for which Z = Sn and In. These alloys show a martensitic transition in the range of compositions $Ni_{50}Mn_{(50-x)}Z_x$ with $x < 0.25$ (Mn-rich region). The interesting composition range is a narrow interval close to $e/a \simeq 8$ where, on cooling, these systems first become ferromagnetic and, on further cooling, undergo the martensitic transition (see figure 4). In figure 30 we present examples of curves showing the magnetization as a function of temperature, at selected applied fields, over a temperature range which spans the transition region. As in the case of Ni–Mn–Ga alloys, from these curves we can obtain the change of magnetization ΔM which takes place at the transition as a function of H. Results are given in figure 31 for $Ni_{50}Mn_{35}Sn_{15}$ and $Ni_{50}Mn_{34}In_{16}$. In these systems, ΔM decreases with increasing field until a negative saturation value is reached at a rather low field. This behaviour is essentially different from that described above for Ni–Mn–Ga. It has been suggested [120] that the almost monotonic decrease displayed by ΔM is a consequence of a low magnetic anisotropy in the martensitic phase. This point needs, however, further confirmation since magnetic anisotropy of the martensitic phase has not been, to our knowledge, reported for these alloy families. It is interesting to point out that some results indirectly support this interpretation. In particular, the fact that no twin boundary motion occurs in this class of alloys as discussed in section 4.4. In the case of the $Ni_{50}Mn_{35}Sn_{15}$, results depicted in figure 31 show that the saturation value of ΔM is not rigorously approached in a monotonic way. Instead, a weak minimum occurs, and by further increasing the field, ΔM slightly increases towards the negative saturation value. This could indicate that while the influence of magnetic anisotropy (extrinsic effect) is weak, it is not strictly negligible.

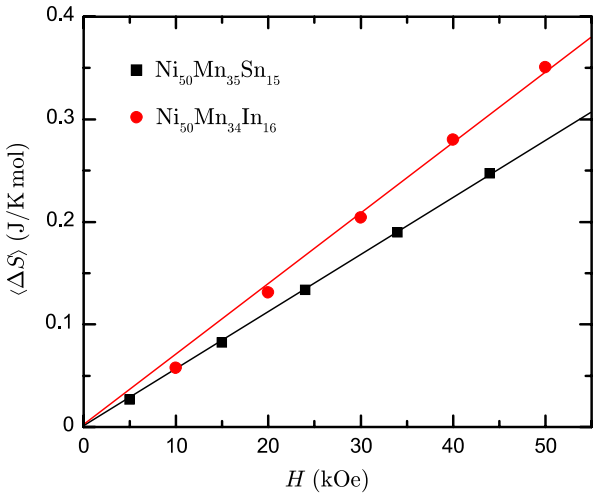

Figure 32. Average field-induced entropy change, $\langle \Delta S \rangle$, as a function of the applied field H for $Ni_{50}Mn_{35}Sn_{15}$ and $Ni_{50}Mn_{34}In_{16}$. The continuous lines are linear fits.

In the results shown in figure 30, the most relevant feature is the fact that the magnetic moment of the martensitic phase is lower than the magnetic moment of the cubic parent phase (see also figure 5(c)). This can be ascribed to the presence

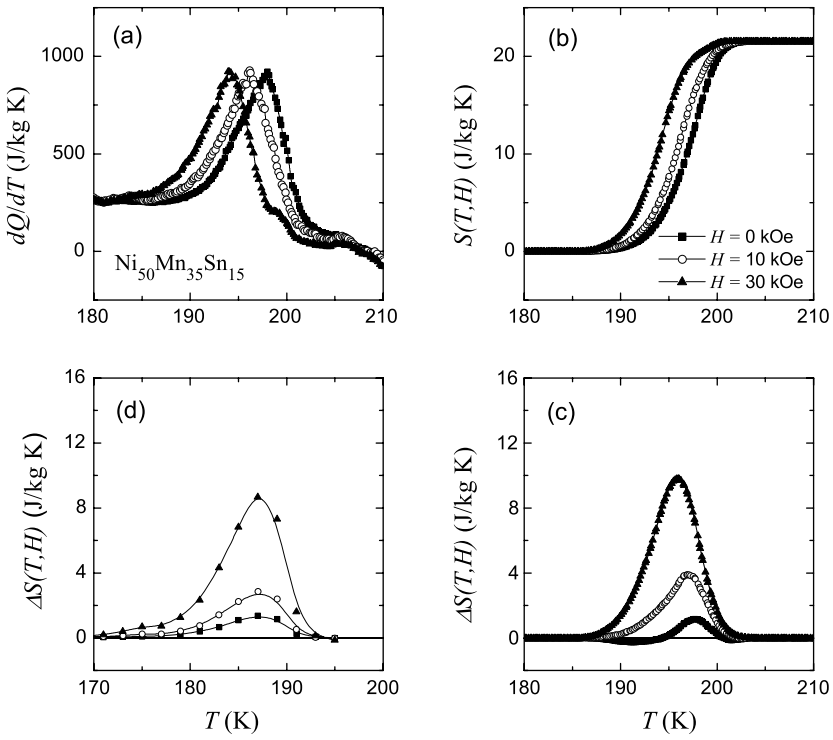

Figure 33. (a) Calorimetric curves (heating runs) for selected values of the applied magnetic field in the range of the martensitic transition in $Ni_{50}Mn_{35}Sn_{15}$. (b) Entropy versus temperature for the three different values of the applied field. (c) Temperature dependence of the (inverse) magnetocaloric effect $\Delta S = \Delta S(H) - \Delta S(0)$ obtained from the $S(T, H)$ curves. (d) Magnetocaloric effect calculated from magnetization measurements. In (c) and (d) data correspond to the following applied fields (from bottom to top): 5, 10 and 30 kOe.

of coexisting antiferromagnetic interactions as discussed in section 3.1.

For Ni–Mn–Ga, to our knowledge, no systematic study of the magnetic properties along the $Ni_{50}Mn_{25+x}Ga_{25-x}$ composition line has been reported, which could serve as a reference to compare results presented for the other Ni–Mn–Z families. Some reports on samples belonging to the $Ni_{50-x}Mn_{25+x}Ga_{25}$ composition line indicate that the magnetic moment of the martensitic phase decreases with increasing x [121], reflecting an enhancement in the antiferromagnetic exchange. On the other hand, the magnetization versus temperature curves do not exhibit a sharp change of magnetization at the martensitic transition temperature. Although for $x = 25$ (Mn_2NiGa) the magnetization of martensite is slightly lower than in the austenite [121], for $x = 5$ it is the martensitic phase which has a slightly higher magnetization [122].

The average field-induced entropy change computed for $Ni_{50}Mn_{35}Sn_{15}$ and $Ni_{50}Mn_{34}In_{16}$ is shown in figure 32. Consistent with the behaviour of ΔM (see figure 31), an inverse magnetocaloric effect is obtained. The average field-induced entropy change linearly increases with increasing H and there is no tendency to saturation which should occur at much higher fields. In this case, the magnetocaloric properties are controlled by the intrinsic microscopic coupling related to the change of magnetic moment induced by the symmetry change taking place at the martensitic transition.

5.3. Comparison of the magnetocaloric effects obtained by different measurement techniques

So far, magnetocaloric properties have been analysed from the field-induced isothermal entropy change obtained from magnetization measurements. As explained in section 2.3, the entropy change can be obtained by several methods. It is thus interesting to compare the results obtained from these different experimental techniques with particular emphasis in calorimetric and thermometric techniques.

Since in Heusler alloys the martensitic transition spreads over a rather large range of temperatures, direct determination of the field-induced entropy change through isothermal calorimetric measurements during field-inducing the transition is difficult. Instead, applying selected constant fields and inducing the transition by changing the temperature provides more reliable results. This technique has been used to study the magnetocaloric effect in $Ni_{50}Mn_{35}Sn_{15}$ [107]. Figure 33(a) shows DSC heating runs under selected magnetic fields. A clear shift in the transition towards lower temperatures with increasing magnetic field is apparent. From DSC curves, the variation of the entropy associated with the transition (referred to the entropy of the low-temperature phase) can be computed as

$$S(T, H) = \int_{A_s}^{T} \frac{1}{T}\left(\frac{dq}{dT}\right) dT, \qquad (27)$$

where $dq/dT = (dq/dt)/(dT/dt)$, with dq/dt being the heat flux and dT/dt the temperature heating rate. T is a temperature within the coexistence region ranging between A_s and A_f. It

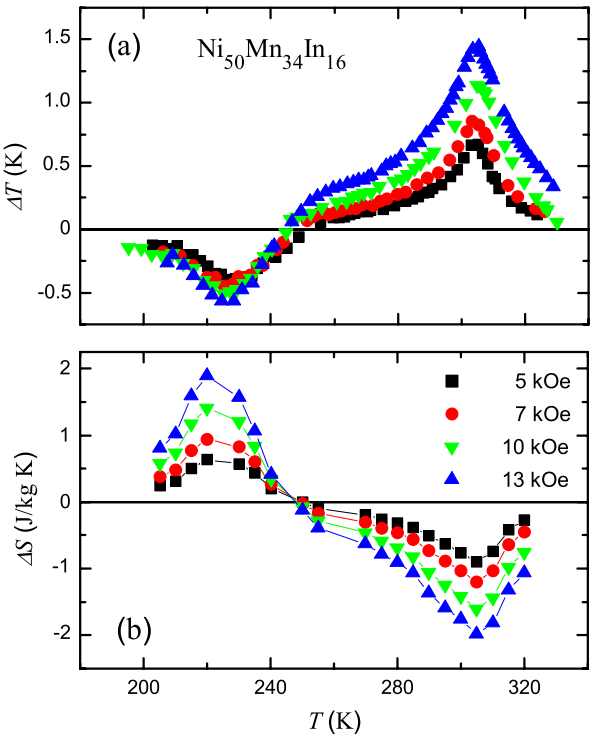

Figure 34. (a) Measured adiabatic temperature change and (b) isothermal entropy change obtained from magnetization isotherms as a function of temperature and selected values of the applied magnetic field.

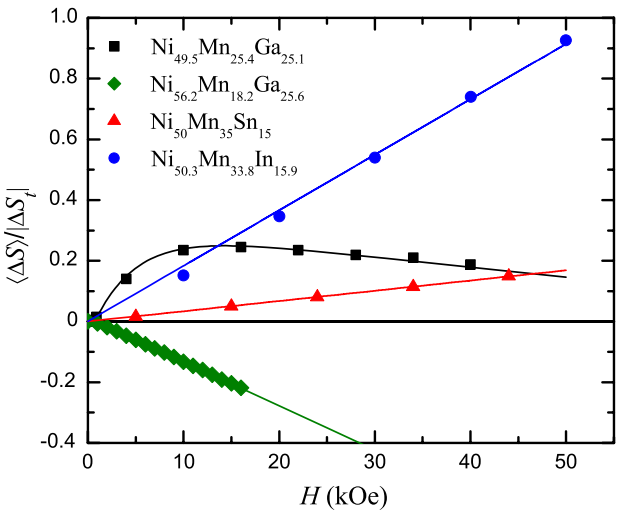

Figure 35. Ratio of the average field-induced entropy and transition entropy changes as a function of the applied magnetic field for $Ni_{49.5}Mn_{25.4}Ga_{25.1}$, $Ni_{56.2}Mn_{18.2}Ga_{25.6}$, $Ni_{50}Mn_{35}Sn_{15}$ and $Ni_{50}Mn_{33.8}In_{15.9}$ Heusler alloys. Transition entropy changes for these four systems are: $|\Delta S_t| = 0.55, 1.42, 1.66, 0.38$ J mol^{-1} K^{-1}, respectively.

was obtained that the whole transition entropy change ΔS_t remains independent of the applied field within the errors. From the $S(T, H)$ curves displayed in figure 33(b), the field-induced entropy change as a function of T for a change of the field from 0 to H can be obtained as

$$\Delta S(T, H) = S(T, H) - S(T, H = 0). \qquad (28)$$

Results are shown in figure 33(c) and are compared with the corresponding field-induced entropy change obtained from magnetization data taken during cooling runs (figure 33(d)). Interestingly, the values of the field-induced entropy change obtained from both methods agree quite well. The small shift in temperature is due to the hysteresis between cooling and heating runs (note the change of the abscissa scale in figure 33(d)). Moreover, the maximum values of the peaks are slightly larger in the case of field-induced entropy changes obtained from calorimetric curves. This is in agreement with inequality (18). Therefore, this small difference could be due to dissipative effects.

Reports on direct measurements of the field-induced adiabatic change of temperature (ΔT_{ad}) are scarce. Measurements of ΔT_{ad} have been conducted with a thermocouple in direct contact with the sample in Ni–Mn–Ga alloys with martensitic and Curie temperatures close to each other [123, 124]. The temperature dependence of ΔT_{ad} is in qualitative agreement with that exhibited by ΔS, but the measured values are significantly lower than those computed from entropy and specific heat data. For the Ni–Mn–In system, magnetization, specific heat and direct temperature measurements were conducted on a series of isoelectronic Ga-doped Ni–Mn–In compounds, [39, 53]. In those measurements, the thermocouple was embedded into the sample. In figure 34, we show the temperature dependence of the field-induced adiabatic temperature change for selected values of the magnetic field in $Ni_{50}Mn_{34}In_{16}$. Temperature changes are compared with the isothermal field-induced entropy change obtained from magnetization data. Results correspond to a broad temperature range that includes the martensitic and the ferromagnetic–paramagnetic transition. The magnetocaloric effect is inverse in the vicinity of the martensitic transition where cooling occurs by magnetization, while it is conventional about the Curie point. The adiabatic temperature change can also be estimated from the field-induced entropy change as $\Delta T = T\Delta S/C$. This expression assumes that the adiabatic process occurs in strict equilibrium. ΔT obtained from direct measurements can actually be identified with ΔT^{irr}. Therefore, any discrepancy between estimations based on the previous expression and direct measurements should be ascribed to dissipative effects during the process. According to equation (19), for increasing H we expect $\Delta T \geqslant T\Delta S/C$. Results reported in [39] are consistent with this prediction.

5.4. Comparing the magnetocaloric effect in different Heusler alloys

It is interesting to compare the average field-induced entropy change in the different classes of magnetic shape-memory materials discussed above. This is shown in figure 35 for nearly stoichiometric Ni_2MnGa (alloy 1 in table 1), $Ni_{56.2}Mn_{18.2}Ga_{25.6}$ (alloy 5 in table 1), $Ni_{50}Mn_{35}Sn_{15}$ and $Ni_{50}Mn_{34}In_{16}$. We have plotted the ratio $\mathcal{R}$ of the average field-induced entropy and the transition entropy changes as a function of the applied magnetic field. The transition

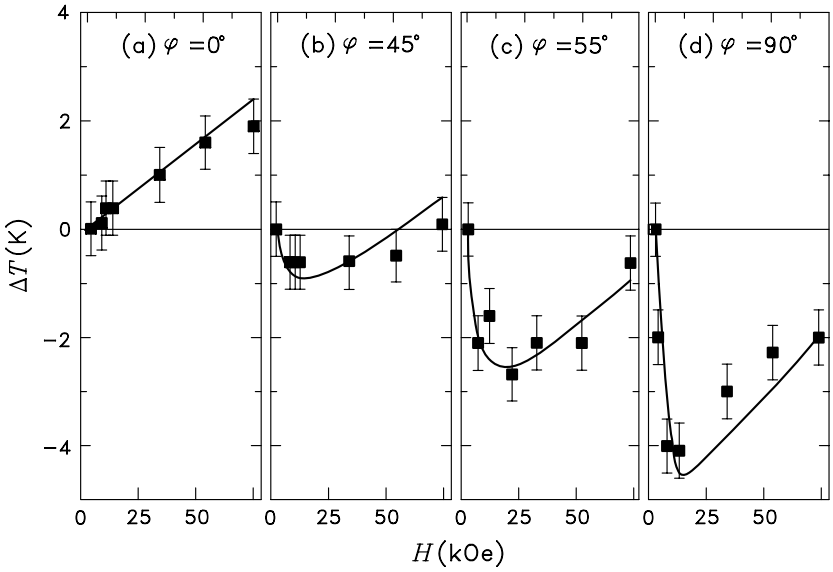

Figure 36. Change ΔT of the reverse martensitic transition temperature A_f in a single-crystal single-variant Ni_2MnGa alloy as a function of an applied magnetic field forming selected angles φ with the magnetization easy axis. (a) $\varphi = 0°$, (b) $\varphi = 45°$, (c) $\varphi = 55°$ and (d) $\varphi = 90°$. Adapted from [125].

entropy change is a measure of the maximum entropy change associated with the transition. Therefore, $\mathcal{R}$ represents the fraction of this maximum amount that can be induced by means of a given applied field. Except for the nearly stoichiometric Ni_2MnGa system, $\mathcal{R}$ varies linearly with the field. It decreases for Ni–Mn–Ga (conventional magnetocaloric behaviour) and increases for Ni–Mn–Sn and Ni–Mn–In (inverse magnetocaloric effect). Taking into account equations (14) and (15), we obtain that $\mathcal{R}$ is related to the shift in the transition temperature with the field through

$$\mathcal{R} = \frac{\langle \Delta S(H) \rangle}{|\Delta S_t|} = -\frac{\Delta T_t(H)}{|\overline{\Delta T}|}. \qquad (29)$$

This is an interesting equation, which indicates that the fraction of induced entropy change crucially depends on the temperature range over which the transition extends ($\overline{\Delta T}$). Results shown in figure 35 should be compared with those giving the change of transition temperature with the applied field for alloys of the same compositions (shown in figure 20). Comparison of these two figures shows that the behaviour of $\Delta T_t(H)$ parallels that of $\mathcal{R}$. This finding corroborates the assertion that the linear decrease of $\mathcal{R}$ with increasing H in non-stoichiometric Ni–Mn–Ga is determined by the fact that the magnetic moment is larger in the martensitic phase than in the cubic phase. By contrast, in Ni–Mn–Sn and Ni–Mn–In the magnetic moment is larger in the cubic phase, and consequently $\mathcal{R}$ linearly increases with increasing H. In the case of nearly stoichiometric Ni–Mn–Ga, the field dependence of ΔT_t and $\mathcal{R}$ is controlled by the magnetocrystalline anisotropy of the martensitic phase. Recent results reported in [125] have clarified the role of the magnetic anisotropy on the field dependence of the martensitic transition temperature. As illustrated from figure 36, starting from a single-variant martensite[9], the reverse transition temperature A_s was measured for a field **H** applied forming selected angles φ with the magnetization easy axis of the martensite. When the field is parallel to the easy axis ($\varphi = 0$), A_s linearly increases with H. By contrast, when it is not parallel, A_s decreases in the low-field region, reaches a minimum and increases on further increasing H. The largest decrease is observed for $\varphi = \pi/2$. The authors have shown that the obtained results can be accounted for by the Clausius–Clapeyron equation when the magnetization change at the transition as a function of H and φ is known. Indeed, the reported results confirm the physical picture discussed in section 5.1 describing the effect of magnetic anisotropy on the structural transition.

6. Summary and perspectives

In this paper, we have reviewed the magnetocaloric properties associated with the martensitic transition undergone by Ni–Mn-based Heusler alloys. Large magnetocaloric effects occur in those alloys in which the Curie point lies above (or is coincident with) the martensitic transition temperature. Moreover, associated with the martensitic transition, these materials display interesting magnetomechanical memory properties such as the magnetic shape-memory effect and magnetic superelasticity, both related to the possibility of magnetically field-inducing large recoverable deformations. These properties are a consequence of the existence of strong interplay between structure and magnetism in this class of materials. Actually, the competition between different ordering modes is a subject of both basic and applied interest in systems

[9] A nearly stoichiometric sample of 3 mm × 1 mm × 0.2 mm with the longest edge cut parallel to the $[001]_P$ direction of the parent (cubic) phase was used. A single-variant martensite was obtained by cooling the sample subjected to either a magnetic field or to a compressive stress parallel to the $[001]_P$ direction.

undergoing solid–solid phase transitions. In the present review, we show that the main features of this interplay are reflected by unusual magnetocaloric properties displayed by these systems.

The obvious consequence of the structural change at the martensitic transition is a modification in the magnetic exchange, thereby leading to different magnetic moments in the two structural phases. Such an intrinsic effect affects the relative phase stability in the presence of an applied magnetic field in such a way that the phase with higher magnetic moment will be stabilized by the field. In Ni–Mn–Ga, the magnetic moment of the martensite is larger than that of the parent phase, which gives rise to a conventional magnetocaloric effect. By contrast, in other Ni–Mn–Z Heusler alloys (with Z as Sn, In, Sb), the magnetic moment of the martensite is lower than that of the parent phase. This drop in magnetization is due to transition-induced antiferromagnetism which originates from the excess of Mn atoms with respect to the 2–1–1 stoichiometry. In these materials, the magnetocaloric effect is inverse, which means that cooling occurs by adiabatic magnetization.

In addition to the afore-mentioned intrinsic magnetostructural coupling, there is also an extrinsic coupling taking place at a mesoscopic scale, related to the existence of magnetic and structural (martensitic variants) domains. Such a coupling becomes relevant when the magnetocrystalline anisotropy of the martensite is large. This occurs in nearly stoichiometric Ni_2MnGa for which there is a decrease of magnetization at the martensitic transition for low applied magnetic fields, which results in an inverse magnetocaloric effect. This extrinsic contribution weakens with increasing magnetic field. For Ni–Mn–Z alloys with excess of Mn this contribution has been found to be irrelevant.

The magnetostructural coupling at both microscopic and mesoscopic length scales provides the basic mechanism for the magnetomechanical properties. While magnetic superelasticity relies upon a strong intrinsic coupling, for the magnetic shape-memory effect to occur, strong extrinsic coupling is needed. It is worth pointing out that the drop of magnetization upon cooling can be compared with the well-known increase of molar volume which takes place when water freezes. Associated with this volume increase, an inverse barocaloric effect is expected to occur. While in the Heusler systems the coexistence of ferro- and antiferromagnetism leads to frustration effects and a high degeneracy of the ground state, the increase of volume in ice is also related to a certain kind of geometrical frustration effect which leads to a highly degenerated ground state [126].

With regards to the potential use of Heusler alloys in technological applications, the magnitude of the magnetocaloric effect found for a number of these materials is competitive when compared to other materials which are being investigated for room temperature refrigeration [7]. It is worth stressing, however, that the materials reviewed here display the following unique features: inverse magnetocaloric effect and giant magnetic-field-induced strains. These two effects are concomitant in a given sample and therefore these materials exhibit multifunctional response to an externally applied field. Thus, specific devices can be envisaged which take advantage of such a multifunctionality.

Acknowledgments

We are grateful to our colleagues J Marcos, X Moya, T Krenke, E Duman, S Aksoy and E F Wassermann for a long-standing collaboration on the topics reviewed in this paper. We acknowledge the financial support from CICyT (Spain) through project MAT2007-62100, DURSI (Generalitat de Catalunya) through project 2005SGR00969 and Deutsche Forschungsgemeinschaft (SPP1239).

References

[1] Tishin A M 1999 Magnetocaloric effect in the vicinity of magnetic phase transitions *Handbook of Magnetic Materials* vol 12, ed K H J Buschow (Amsterdam: Elsevier Science) pp 395–524

[2] Warburg E 1981 Magnetiche Untersuchungen *Ann. Phys.* **13** 141–64

[3] Debye P 1926 Einige Bemerkungen zur Magnetisierung bei tiefer Temperatur *Ann. Phys.* **81** 1154–60

[4] Giauque W F 1927 A thermodynamic treatment of certain magnetic effects. A proposed method of producing temperatures considerably below 1° absolute *J. Am. Chem. Soc.* **49** 1864–70

[5] Giauque W F and MacDougall D P 1933 Attainment of temperatures below 1° absolute by demagnetization of $Gd_2(SO_4)_3{\cdot}8H_2O$ *Phys. Rev.* **43** 768

[6] Pecharsky V K and Gschneider K A 1997 Giant magnetocaloric effect in $Gd_5(Si_2Ge_2)$ *Phys. Rev. Lett.* **78** 4494–7

[7] Brück E 2008 Magnetocaloric refrigeration at ambient temperature *Handbook of Magnetic Materials* vol 17, ed K H J Buschow (Amsterdam: Elsevier Science) pp 235–91

[8] Ziebeck K A and Neumann K U 2001 *Magnetic Properties of Metals* (*Landolt-Bornstein* III/vol 32, Supl. vol 19, subvol. c) (Berlin: Springer-Verlag)

[9] Ullakko K, Huang J K, Kantner C, O'Handley R C and Kokorin V V 1996 Large magnetic-field-induced strains in Ni_2MnGa single crystals *Appl. Phys. Lett.* **69** 1966–8

[10] Hu F, Shen B and Sun J 2000 Magnetic entropy change in $Ni_{51.5}Mn_{22.7}Ga_{25.8}$ alloy *Appl. Phys. Lett.* **76** 3460–2

[11] Hu F, Shen B, Sun J and Wu G 2001 Large magnetic entropy change in a Heusler alloy $Ni_{52.6}Mn_{23.1}Ga_{24.3}$ single crystal *Phys. Rev.* B **64** 132412

[12] Marcos J, Planes A, Mañosa L, Casanova F, Batlle X and Labarta A 2002 Magnetic field induced entropy change and magnetoelasticity in Ni–Mn–Ga alloys *Phys. Rev.* B **66** 224413

[13] Marcos J, Mañosa L, Planes A, Casanova F, Batlle X and Labarta A 2003 Multiscale origin of the magnetocaloric effect in Ni–Mn–Ga shape-memory alloys *Phys. Rev.* B **68** 094401

[14] Pareti L, Solzi M, Albertini F and Paoluzi A 2003 Giant entropy change at the co-occurrence of structural and magnetic transitions in the $Ni_{2.19}Mn_{0.81}Ga$ Heusler alloy *Eur. Phys. J.* B **32** 303–7

[15] Annaorazov M P, Nikitin S A, Tyurin A L, Asatryan K A and Dovletov A Kh 1996 Anomalously high entropy change in FeRh alloy *J. Appl. Phys.* **79** 1689–95

[16] Krenke T, Duman E, Acet M, Wassermann E F, Moya X, Mañosa L and Planes A 2005 Inverse magnetocaloric effect in ferromagnetic Ni–Mn–Ga *Nat. Mater.* **4** 450–4

[17] Mischenko A S, Zhang Q, Scott J F, Whatmore R W and Mathur N D 2006 Giant electrocaloric effect in thin-film $PbZr_{0.95}Ti_{0.05}O_3$ *Science* **311** 1270–1

[18] Strässle T, Furrer A, Hossain Z and Geibel Ch 2003 Magnetic cooling by the application of external pressure in rare-earth compounds *Phys. Rev.* B **67** 054407

[19] Bonnot E, Romero R, Vives E, Mañosa L and Planes A 2008 Elastocaloric effect associated with the martensitic transition in shape-memory alloys *Phys. Rev. Lett.* **100** 125901

[20] Dan'kov S Y, Tishin A M, Pecharsky V K and Gschneidner K A 1998 Magnetic phase transitions and the magnetothermal properties of gadolinium *Phys. Rev.* B **57** 3478–90

[21] Tolédano J C and Tolédano P 1987 *The Landau Theory of Phase Transitions* (Singapore: World Scientific)

[22] Triguero C, Porta M and Planes A 2007 Magnetocaloric effect in metamagnetic systems *Phys. Rev.* B **76** 094415

[23] Bean C P and Rodbell D S 1962 Magnetic disorder as a first-order phase transformation *Phys. Rev.* **126** 104–15

[24] Tishin A M, Gschneidner K A and Pecharsky V K 1999 Magnetocaloric effect and heat capacity in the phase-transition region *Phys. Rev.* B **59** 503–11

[25] Giguère A, Földeàki M, Ravi Gopal S, Chahine R, Bose T K, Frydman A and Barclay J A 1999 Direct measurement of the 'giant' adiabatic temperature change in $Gd_5Si_2Ge_2$ *Phys. Rev. Lett.* **83** 2262–5

Gschneider K A, Pecharsky V K, Brük E, Duijn H G and Levin E M 2000 Comment on direct measurement of the 'giant' adiabatic temperature change in $Gd_5Si_2Ge_2$ *Phys. Rev. Lett.* **85** 4190

Sun J R, Hu F X and Shen B J 2000 Comment on direct measurement of the 'giant' adiabatic temperature change in $Gd_5Si_2Ge_2$' *Phys. Rev. Lett.* **85** 4191

Földeàki M F, Chahine R, Bose T K and Barclay J A 2000 Reply *Phys. Rev. Lett.* **85** 4192

[26] Ortín J, Planes A and Delaey L 2006 Hysteresis in shape-memory materials *The Science of Hysteresis* vol III, ed G Bertotti and I Mayergoyz (Oxford: Academic) pp 467–553 and references therein

[27] Pérez-Reche F J, Vives E, Mañosa L and Planes A 2001 Athermal character of structural phase transitions *Phys. Rev. Lett.* **87** 195701

[28] Pérez-Reche F J, Stipcich M, Vives E, Mañosa L, Planes A and Morin M 2004 Kinetics of martensitic transitions in Cu-Al-Mn under thermal cycling: analysis at multiple length scales *Phys. Rev.* B **69** 064101

[29] Pecharsky V K and Gschneidner K A 1999 Magnetocaloric effect from indirect measurements: magnetization and heat capacity *J. Appl. Phys.* **86** 565–75

[30] Casanova F, Batlle X, Labarta A, Marcos J, Mañosa L and Planes A 2002 Entropy change and magnetocaloric effect in $Gd_5(Si_xGe_{1-x})_4$ *Phys. Rev.* B **66** 100401(R)

[31] Tocado L, Palacios E and Burriel R 2005 Direct measurement of the magnetocaloric effect in $Tb_5Si_2Ge_2$ *J. Magn. Magn. Mater.* **290/291** 719–22

[32] Plackowski T, Wang Y and Junod A 2002 Specific-heat and magnetocaloric effect measurements using commercial heat-flow sensors *Rev. Sci. Instrum.* **73** 2755–65

[33] Marcos J, Casanova F, Batlle X, Labarta A, Planes A and Mañosa L 2003 A high-sensitivity differential scanning calorimeter with magnetic field for magnetostructural transitions *Rev. Sci. Instrum.* **73** 4768–71

[34] Basso V, Kupferling M, Sasso C P and Giudici L 2008 A peltier cell calorimeter for the direct measurement of the isothermal entropy change in magnetic materials *Rev. Sci. Instrum.* **79** 063907

[35] Jeppesen S, Linderoth S, Pryds N, Theil Kuhn L and Buch Jensen J 2008 Indirect measurement of the magnetocaloric effect using a novel differential scanning calorimeter with magnetic field *Rev. Sci. Instrum.* **79** 083901

[36] Miyoshi Y, Morrison K, Moore J D, Caplin A D and Cohen L F 2008 Heat capacity and latent heat measurements on CoMnSi using a microcalorimeter *Rev. Sci. Instrum.* **79** 074901

[37] Casanova F, Labarta A, Batlle X, Pérez-Reche F J, Mañosa L and Planes A 2005 Direct observation of the magnetic-field-induced entropy change in $Gd_5(Si_xGe_{1-x})_4$ giant magnetocaloric alloys *Appl. Phys. Lett.* **86** 262504

[38] Dinesen A R, Linderoth S and Mørup S 2005 Direct and indirect measurement of the magnetocaloric effect in $La_{0.67}Ca_{0.33-x}Sr_xMnO_{3\pm\delta}$ ($x \in [0; 0.33]$) *J. Phys.: Condens. Matter* **17** 6257–69

[39] Moya X, Mañosa L, Planes A, Aksoy S, Acet M, Wassermann E F and Krenke T 2007 Cooling and heating by adiabatic magnetization in the $Ni_{50}Mn_{34}In_{16}$ magnetic shape-memory alloy *Phys. Rev.* B **75** 184412

[40] Levitin R Z, Snegirev V V, Kopylov A V, Lagutin A S and Gerber A 1997 Magnetic method of magnetocaloric effect determination in high pulsed magnetic fields *J. Magn. Magn. Mater.* **170** 223–7

[41] Webster P J, Ziebeck K R A, Town S L and Peak M S 1984 Magnetic order and phase transformation in Ni_2MnGa *Phil. Mag.* B **49** 295–310

[42] Ranjan R, Banik S, Barman S R, Kumar U, Mukhopadhyay P K and Pandey D 2006 Powder x-ray diffraction study of the thermoelastic martensitic transition in $Ni_2Mn_{1.05}Ga_{0.95}$ *Phys. Rev.* B **74** 224443

[43] Krenke T, Acet M, Wassermann E F, Moya X, Mañosa L and Planes A 2005 Martensitic transitions and the nature of ferromagnetism in the austenitic and martensitic states of Ni–Mn–Sn alloys *Phys. Rev.* B **72** 014412

[44] Krenke T, Acet M, Wassermann E F, Moya X, Mañosa L and Planes A 2006 Ferromagnetism in the austenitic and martensitic states of Ni–Mn–In alloys *Phys. Rev.* B **73** 174413

[45] Aksoy S, Krenke T, Acet M, Wassermann E F, Moya X, Mañosa L and Planes A 2007 Magnetization easy axis in martensitic Heusler alloys estimated by strain measurements under magnetic field *Appl. Phys. Lett.* **91** 251915

[46] Sutou Y, Imano Y, Koeda N, Omori T, Kainuma R, Ishida K and Oikawa K 2004 Magnetic and martensitic transformations of NiMnX (X = In, Sn, Sb) ferromagnetic shape memory alloys *Appl. Phys. Lett.* **85** 4358–60

[47] Wachtel E, Henninger F and Predel B 1983 Constitution and magnetic properties of Ni–Mn–Sn alloys—solid and liquid state *J. Magn. Magn. Mater.* **38** 305–15

[48] Marcos J 2004 *PhD Thesis* Universitat de Barcelona, Barcelona

[49] Righi L, Albertini F, Vila E, Paoluzi A, Calestani G, Chernenko V, Besseghini S, Ritter C and Passaretti F 2008 Crystal structure of 7 M modulated Ni–Mn–Ga martensitic phase *Acta Mater.* **56** 4529–35

[50] Brown P J, Gandy A P, Kanomata T, Matsumoto M, Neumann K U, Sheikh A and Ziebeck K R A 2008 The crystal structure and transformation mechanisms in stoichiometric Ni_2MnGa *Mater. Sci. Forum* **583** 285–301

[51] Acet M, Duman E, Wassermann E F, Mañosa L and Planes A 2002 Coexisting ferro- and antiferromagnetism in Ni_2MnAl alloys *J. Appl. Phys.* **92** 3867–71

[52] Krenke T, Moya X, Aksoy S, Acet M, Entel P, Mañosa L, Planes A, Elerman Y, Yücel A and Wassermann E F 2007 Electronic aspects of the martensitic transition in Ni–Mn based Heusler alloys *J. Magn. Magn. Mater.* **310** 2788–9

[53] Aksoy S, Krenke T, Acet M, Wassermann E F, Moya X, Mañosa L and Planes A 2007 Tailoring magnetic and magnetocaloric properties of martensitic transitions in ferromagnetic Heusler alloys *Appl. Phys. Lett.* **91** 241916

[54] Krenke T 2007 *PhD Thesis* Universität Duisburg-Essen, Duisburg

[55] Krén E, Nagy E, Nagy I, Pál L and Szabò P 1968 Structures and phase transformations in the Mn–Ni system near equiatomic concentration *J. Phys. Chem. Solids* **29** 101–8

[56] Galanakis I and Dederichs P H 2002 Slater–Pauling behavior and origin of the half-metallicity of the full-Heusler alloys *Phys. Rev.* B **66** 174429

[57] Galanakis I, Dederichs P H and Papanikolaou N 2002 Origin and properties of the gap in the half-ferromagnetic Heusler alloys *Phys. Rev.* B **66** 134428

[58] Galanakis I, Şaşioğlu E and Özdoan K 2008 Magnetic phase transition in half-metallic CoMnSb and NiMnSb semi-Heusler alloys upon Cu doping: first-principles calculations *Phys. Rev.* B **77** 214417

[59] Enkovaara J, Heczko O, Ayuela A and Nieminen R M 2003 Coexistence of ferromagnetic and antiferromagnetic order in Mn-doped Ni_2MnGa *Phys. Rev.* B **67** 212405

[60] Helmholdt R B, de Groot R A, Mueller F M, van Engen P G and Buschow K H J 1984 Magnetic and crystallographic properties of several $C1_b$ type Heusler compounds *J. Magn. Magn. Mater.* **43** 249–55

[61] Murakami Y, Watanabe Y, Kanaizuka T and Kachi S 1981 Magnetic properties and phase change of $Ni_{3-y}Mn_ySn$ alloy *Trans. Japan. Inst. Met.* **22** 551–7

[62] Kanomata T, Shirikawa K and Kaneko T 1987 Effect of hydrostatic pressure on the Curie temperature of the Heusler alloys Ni_2MnZ (Z = Al, Ga, Sn and Sb) *J. Magn. Magn. Mater.* **65** 76–82

[63] Stager C V and Campbell C C M 1978 Antiferromagnetic order in the Heusler alloy, $Ni_2Mn(Mn_xSn_{1-x})$ *Can. J. Phys.* **56** 674–7

[64] Buschow K H J, van Engen P G and de Mooij D B 1984 Magnetic and magneto-optical properties of Heusler alloys of the type $Ni_{3-x}Mn_x$ *J. Magn. Magn. Mater.* **40** 339–47

[65] Sobczak R 1981 Magnetic properties of Heusler alloys $Ni_{3-x}Mn_xSn$ *J. Magn. Magn. Mater.* **24** 325–7

[66] Helmholdt R B and Buschow K H J 1987 Crystallographic and magnetic structure of Ni_2MnSn and $NiMn_2Sn$ *J. Less-Common Met.* **128** 167–71

[67] Szytuła A, Kołodziejczyk A, Rżany H and Todorović Wanic A 1972 Atomic and magnetic structure of the Heusler alloys Ni_2MnSb, Ni_2MnSn, Co_2MnSn *Phys. Status Solidi* a **10** 57–65

[68] Castelliz L 1951 Eine ferromagnetische phase im system nickel-mangan-antimon *Monatsh. Chem.* **82** 1059–85

[69] Enkovaara J, Ayuela A, Nordström L and Nieminen R M 2002 Magnetic anisotropy in Ni_2MnGa *Phys. Rev.* B **65** 134422

[70] Tickle R and James R D 1999 Magnetic and magnetomechanical properties of Ni_2MnGa *J. Magn. Magn. Mater.* **195** 627–38

[71] O'Handley R C, Murray S J, Marioni M, Nembach H and Allen S M 2000 Phenomenology of giant magnetic-field-induced strain in ferromagnetic shape-memory materials *J. Appl. Phys.* **87** 4712–7

[72] Wirth S, Leithe-Jasper A, Vasil'ev A N and Coey J M D 1997 Structural and magnetic properties of Ni_2MnGa *J. Magn. Magn. Mater.* **167** L7–11

[73] Albertini F, Morellon L, Algarabel P A, Ibarra M R, Pareti L, Arnold Z and Calestani G 2001 Magnetoelastic effects and magnetic anisotropy in Ni_2MnGa polycrystals *J. Appl. Phys.* **89** 5614–7

[74] Albertini F, Pareti L, Paoluzi A, Morellon L, Algarabel P A, Ibarra M R and Righi L 2002 Composition and temperature dependence of the magnetocrystalline anisotropy in $Ni_{2+x}Mn_{1+y}Ga_{1+z}$ $(x + y + z = 0)$ Heusler alloys *Appl. Phys. Lett.* **81** 4032–4

[75] Albertini F, Solzi M, Paoluzi A and Righi L 2008 Magnetocaloric properties and magnetic anisotropy by tailoring phase transitions in NiMnGa alloys *Mater. Sci. Forum* **583** 169–96

[76] Khan M, Dubenko I, Stadler S and Ali N 2007 Exchange bias in bulk Mn rich Ni–Mn–Sn Heusler alloys *J. Appl. Phys.* **102** 113914

[77] Li Z, Jing C, Chen J, Yuan S, Cao S and Zhang J 2007 Observation of exchange bias in the martensitic state of $Ni_{50}Mn_{36}Sn_{14}$ Heusler alloy *Appl. Phys. Lett.* **91** 112505

[78] Yu S Y, Ma L, Liu G D, Liu Z H, Chen J L, Cao Z X, Wua G H, Zhang B and Zhang X X 2007 Magnetic field-induced martensitic transformation and large magnetoresistance in NiCoMnSb alloys *Appl. Phys. Lett.* **90** 242501

[79] Koyama K, Okada H, Watanabe K, Kanomata T, Kainuma R, Ito W, Oikawa K and Ishida K 2006 Observation of large magnetoresistance of magnetic Heusler alloy $Ni_{50}Mn_{36}Sn_{14}$ in high magnetic fields *Appl. Phys. Lett.* **89** 182510

[80] Brown P J, Grandy A P, Ishida K, Kainuma R, Kanomata T, Neumann K-U, Oikawa K, Ouladdiaf B and Ziebeck K R A 2006 The magnetic and structural properties of the magnetic shape memory compound $Ni_2Mn_{1.44}Sn_{0.56}$ *J. Phys.: Condens. Matter* **18** 2249–59

[81] Umetsu R Y, Kainuma R, Amako Y, Taniguchi Y, Kanomata T, Fukushima K, Fujita A, Oikawa K and Ishida K 2008 Mössbauer study on martensite phase in $Ni_{50}Mn^{57}_{36.5}Fe_{0.5}Sn_{13}$ metamagnetic shape memory alloy *Appl. Phys. Lett.* **93** 042509

[82] Aksoy S, Acet M, Deen P, Mañosa L and Planes A 2009 unpublished

[83] Otsuka K and Wayman C M (ed) 1998 *Shape-Memory Materials* (Cambridge: Cambridge University Press)

[84] Chang L C and Read T A 1951 Plastic deformation and diffusionless phase changes in metals—the gold-cadmium beta-phase *Trans. AIME* **189** 47–52

[85] Buehler W J, Gilfrich J W and Wiley R C 1963 Effect of low-temperature phase changes on mechanical properties of alloys near composition TiNi *J. Appl. Phys.* **34** 1475–7

[86] Otsuka K and Kakehita T (ed) 2002 Science and technology of shape-memory alloys: new developments *MRS Bull.* **27** (February) 91

[87] Tickle R, James R D, Shield T, Wuttig M and Kokorin V V 1999 Ferromagnetic shape memory in the NiMnGa system *IEEE Trans. Magn.* **35** 4301–10

[88] Pan Q and James R D 2000 Micromagnetic study of Ni_2MnGa under applied field *J. Appl. Phys.* **87** 4702–6

[89] Lai Y W, Scheerbaum N, Hinz D, Gutfleisch O, Schäfer R, Schultz L and McCord J 2007 Absence of magnetic domain wall motion during magnetic field induced twin boundary motion in bulk magnetic shape memory alloys *Appl. Phys. Lett.* **90** 192504

[90] O'Handley R C 2000 *Modern Magnetic Materials: Principles and Applications* (New York: Wiley)

[91] Sozinov A, Likhachev A A, Lanska N and Ullakko K 2002 Giant magnetic-field-induced strain in NiMnGa seven-layered martensitic phase *Appl. Phys. Lett.* **80** 1746–8

[92] Okamoto N, Fukuda T and Kakeshita T 2008 Temperature dependence of rearrangement of martensite variants by magnetic field in 10 M, 14 M and 2 M martensites of Ni–Mn–Ga alloys *Mater. Sci. Eng.* A **481/482** 306–9

[93] Heczko O 2005 Magnetic shape memory effect and magnetization reversal *J. Magn. Magn. Mater.* **290/291** 787–94

[94] Kakeshita T, Fukuda T and Kakeuchi T 2006 Magneto-mechanical evaluation for twinning plane movement driven by magnetic field in ferromagnetic shape memory alloys *Mater. Sci. Eng.* A **438–440** 12–7

[95] Heczko O, Straka L, Lanska N, Ullakko K and Enkovaara J 2002 Temperature dependence of magnetic anisotropy in Ni–Mn–Ga alloys exhibiting giant field-induced strain *J. Appl. Phys.* **91** 8228–30

[96] Karaca H E, Karaman I, Basaran B, Chumlyakov Y I and Maier H J 2006 Magnetic field and stress induced martensite reorientation in NiMnGa ferromagnetic shape memory alloy single crystals *Acta Mater.* **54** 233–45

[97] Malla A, Dapino M J, Lograsso T A and Schlagel D L 2006 Large magnetically induced strains in $Ni_{50}Mn_{28.7}Ga_{21.3}$ driven with collinear field and stress *J. Appl. Phys.* **99** 063903

[98] Chopra H D, Chunhai J and Kokorin V V 2000 Magnetic-field-induced twin boundary motion in magnetic shape-memory alloys *Phys. Rev.* B **61** R14913–5

[99] Sullivan M R and Chopra H D 2004 Temperature- and field-dependent evolution of micromagnetic structure in ferromagnetic shape-memory alloys *Phys. Rev.* B **70** 094427

[100] Ge Y, Heczko O, Söderberg O and Hannula S P 2006 Magnetic domain evolution with applied field in a Ni–Mn–Ga magnetic shape memory alloy *Scr. Mater.* **54** 2155–60

[101] Brown P J, Dennis B, Crangle J, Kanomata T, Matsumoto M, Neumann K-U, Justham L M and Ziebeck K R A 2004 Stability of martensitic domains in the ferromagnetic alloy Ni_2MnGa: a mechanism for shape memory behaviour *J. Phys.: Condens. Matter* **16** 65–75

[102] Molnar P, Sittner P, Novak V, Prokleska J, Sechovsky V, Ouladdiaf B, Hanulla S P and Heczko O 2008 *In situ* neutron diffraction study of magnetic field induced martensite reorientation in Ni–Mn–Ga under constant stress *J. Phys.: Condens. Matter* **20** 104224

[103] Kainuma R, Imano Y, Ito W, Sutou Y, Oikawa K, Fujita A, Ishida K, Okamoto S, Kitakami O and Kanomata T 2006 Metamagnetic shape memory effect in a Heusler-type $Ni_{43}Co_7Mn_{39}Sn_{11}$ *Appl. Phys. Lett.* **88** 192513

[104] Kainuma R, Imano Y, Ito W, Sutou Y, Morito H, Okamoto S, Kitakami O, Oikawa K, Fujita A, Kanomata T and Ishida K 2006 Magnetic-field-induced shape recovery by reverse phase transition *Nature* **439** 957–60

[105] Kim J H, Inaba F, Fukuda T and Kakeshita T 2006 Effect of magnetic field on martensitic transformation temperature in Ni–Mn–Ga ferromagnetic shape memory alloys *Acta Mater.* **54** 493–9

[106] Jeong S, Inoue K, Inoue S, Koterazawa K, Taya M and Inoue K 2003 Effect of magnetic field on martensite transformation in a polycrystalline Ni_2MnGa *Mater. Sci. Eng.* A **359** 253–60

[107] Moya X, Mañosa L, Planes A, Krenke T, Duman E, Acet M and Wassermann E F 2007 Calorimetric study of magnetocaloric effect in ferromagnetic Ni–Mn–Sn *J. Magn. Magn. Mater.* **316** e572–4

[108] Krenke T, Duman E, Acet M, Wassermann E F, Moya X, Mañosa L, Planes A, Suard E and Ouladdiaf B 2007 Magnetic superelasticity and inverse magnetocaloric effect in Ni–Mn–In *Phys. Rev.* B **75** 104414

[109] Inoue K, Enami K, Yamaguchi Y, Ohoyama K, Morii Y, Matsuoka Y and Inoue K 2000 Magnetic-field-induced martensitic transformation in Ni_2MnGa based alloys *J. Phys. Soc. Japan* **69** 3485–8

[110] Koyama K, Watanabe K, Kanomata T, Kainuma R, Oikawa K and Ishida K 2006 Observation of field-induced reverse transformation in ferromagnetic shape memory alloy $Ni_{50}Mn_{36}Sn_{14}$ *Appl. Phys. Lett.* **88** 132505

[111] Wang Y D, Ren Y, Huang E W, Nie Z H, Wang G, Liu Y D, Deng J N, Zuo L, Choo H, Liaw P K and Brown D E 2007 Direct evidence on magnetic-field-induced phase transition in a NiCoMnIn ferromagnetic shape memory alloy under a stress field *Appl. Phys. Lett.* **90** 101917

[112] Ganor Y, Shilo D, Shield T W and James R 2008 Breaching the work output limitation of ferromagnetic shape memory alloys *Appl. Phys. Lett.* **93** 122509

[113] Pasquale M, Sasso C P, Besseghini S, Villa E and Chernenko V 2002 Temperature dependence of magnetically induced strain in single crystal samples of Ni–Mn–Ga *J. Appl. Phys.* **91** 7815

[114] Chu S-Y, Cramb A, De Graef M, Laughlin D and McHenry M E 2000 The effect of field cooling and field orientation on the martensitic phase transformation in a Ni_2MnGa single crystal *Appl. Phys. Lett.* **87** 5777

[115] Sharma V K, Chattopadhyay M K and Roy S B 2007 Kinetic arrest of the first order austenite to martensite phase transition in $Ni_{50}Mn_{34}In_{16}$: dc magnetization studies *Phys. Rev.* B **76** 140401

[116] Chatterjee S, Giri S, Majumdar S and De S K 2008 Thermo-magnetic irreversibility in $Ni_2Mn_{1.36}Sn_{0.64}$ shape memory alloy *Phys. Rev.* B **77** 224440

[117] Ito W, Ito K, Umetsu R Y, Kainuma R, Koyama K, Watanabe K, Fujita A, Oikawa K, Ishida K and Kanomata T 2008 Kinetic arrest of martensitic transformation in the NiCoMnIn metamagnetic shape memory alloy *Appl. Phys. Lett.* **92** 021908

[118] Hu H, Sun J, Wu G and Shen B 2001 Magnetic entropy change in $Ni_{50.1}Mn_{20.7}Ga_{29.6}$ single crystal *J. Appl. Phys.* **90** 5216–9

[119] Recarte V, Pérez-Landazabal J I, Gómez-Polo C, Cesari E and Dutkiewicz J 2006 Magnetocaloric effect in Ni–Fe–Ga shape-memory alloys *Appl. Phys. Lett.* **88** 132503

[120] Planes A, Mañosa L, Moya X, Marcos J, Acet M, Krenke T, Aksoy S and Wassermann E F 2008 Magnetocaloric and shape-memory properties in magnetic Heusler alloys *Adv. Mater. Res.* **52** 221–8

[121] Liu G D, Dai X F, Yu S Y, Zhu Z Y, Chen J L, Wu G H, Zhu H and Xiao J Q 2006 Physical and electronic structure and magnetism of Mn_2NiGa: experiment and density-functional theory calculations *Phys. Rev.* B **74** 054435

[122] Banik S, Rawat R, Mukhopadhyay P K, Ahuja B L, Chakrabarti A, Paulose P L, Singh S, Singh A K, Pandey D and Barman S R 2008 Magnetoresistance behavior of ferromagnetic shape memory alloy $Ni_{1.75}Mn_{1.25}Ga$ *Phys. Rev.* B **77** 224417

[123] Pasquale M, Sasso C P, Lewis L H, Giudici L, Lograsso T and Schlagel D 2005 Magnetostructural transition and magnetocaloric effect in $Ni_{55}Mn_{20}Ga_{25}$ single crystals *Phys. Rev.* B **72** 094435

[124] Khovaylo V V, Skokov K P, Koshkid'ko Y S, Koledov V V, Shavrov V G, Buchelnikov V D, Taskaev S V, Miki H, Takagi T and Vasiliev A N 2008 Adiabatic temperature change at first-order magnetic phase transitions: $Ni_{2.19}Mn_{0.81}Ga$ as a case study *Phys. Rev.* B **78** 060403(R)

[125] Fukuda T, Maeda H, Yasui M and Kakeshita T 2009 Influence of magnetocrystalline anisotropy on martensitic transformation under magnetic field of single-crystalline Ni_2MnGa *Scr. Mater.* **60** 261–3

[126] Moessner R and Ramirez A P 2006 Geometrical frustration *Phys. Today* **59** (February) 24–9